

1 **FULL TITLE:** The orphan nuclear receptor Nr2f6 impairs skeletal muscle oxidative capacity and  
2 regulates muscle mass in mice.

3 **SHORT TITLE:** Nr2f6 regulates muscle biology

4 **AUTHORS:**

5 Dimitrius Santiago Passos Simões Fróes Guimarães<sup>1,2,\*</sup>

6 Ninon Melany Flores Barrios<sup>1</sup>

7 André Gustavo de Oliveira<sup>1</sup>

8 David Rizo-Roca<sup>2</sup>

9 Maxence Jollet<sup>3</sup>

10 Jonathon A.B. Smith<sup>2</sup>

11 Thiago Reis Araujo<sup>1</sup>

12 Marcos Vinicius da Cruz<sup>1</sup>

13 Emilio Marconato Junior<sup>1</sup>

14 Sandro Massao Hirabara<sup>4</sup>

15 André Schwambach Vieira<sup>1</sup>

16 Anna Krook<sup>2</sup>

17 Juleen R. Zierath<sup>2,3</sup>

18 Leonardo dos Reis Silveira<sup>1</sup>

19

20 **AFFILIATIONS:**

21 <sup>1</sup>Department of Structural and Functional Biology, University of Campinas, Campinas, Brazil

22 <sup>2</sup>Department of Physiology and Pharmacology, Karolinska Institutet, Stockholm, Sweden

23 <sup>3</sup>Department of Molecular Medicine and Surgery, Karolinska Institutet, Stockholm, Sweden

24 <sup>4</sup>Interdisciplinary Post-Graduate Program in Health Sciences, Cruzeiro do Sul University, São Paulo,

25 Brazil

26 **\*Correspondence**

27 Dimitrius Santiago P.S.F. Guimarães

28 Centro de Pesquisa em Obesidade e Comorbidades

29 Universidade Estadual de Campinas - Instituto de Biologia

30 Rua Carl Von Linnaeus - Bloco Z

31 CEP 13083-862

32 Campinas - SP

33 Brazil

34 F: +55 (19) 3521-6191.

35 E-mail: [dimitrius.guimaraes@ki.se](mailto:dimitrius.guimaraes@ki.se); [d211529@unicamp.br](mailto:d211529@unicamp.br)

36

37

38

39

40

41

42

43 **ABSTRACT**

44 The maintenance of skeletal muscle plasticity upon changes in the environment, nutrient supply, and  
45 exercise depends on regulatory mechanisms that couple structural and metabolic adaptations. However,  
46 the transcriptional control of both processes by nuclear receptors (NR) remains underexplored. Nr2f6 is  
47 an orphan NR and a key regulator of metabolism and differentiation. Nonetheless, its role in muscle  
48 biology remains elusive. Here, we report, for the first time, the effects of Nr2f6 modulation in skeletal  
49 muscle *in vivo* and *in vitro*. Depletion of Nr2f6 increased myocyte's oxidative capacity and sharply  
50 attenuated lipid-induced cell death, which was associated with direct derepression of uncoupling protein  
51 3 and PGC-1  $\alpha$  promoters' transactivation. Conversely, Nr2f6 overexpression in the *tibialis anterior*  
52 induced atrophy and hypoplasia, accompanied by impairment of force production and the establishment  
53 of a molecular signature of inflammation, and a decrease in genes involved in oxidative metabolism and  
54 contraction. Additionally, global transcriptomics showed that Nr2f6 upregulated core components of the  
55 cell division machinery and repressed myogenesis genes, thus decoupling myoblast proliferation from  
56 differentiation. Collectively, our findings define a novel role for Nr2f6 as a molecular transducer  
57 maintaining the balance between skeletal muscle contractile function and oxidative capacity, with  
58 implications for metabolic diseases and myopathies treatment.

59 **KEYWORDS:** muscle atrophy; Nr2f6; skeletal muscle; transcription; energy metabolism; nuclear  
60 receptor;

61

## 62 INTRODUCTION

63 Muscle contraction is a highly coordinated process initiated by the transmission of the action potential  
64 from the afferent neurons to the muscle. Subsequent depolarization of the muscle fiber triggers an action  
65 potential that propagates along the sarcolemma, stimulating the release of calcium ions from the  
66 sarcoplasmic reticulum, and ultimately promoting myosin-actin cross-bridge cycling and force  
67 production. This process requires an accessory metabolic machinery to generate the energy needed to  
68 support contraction, and disruption in either muscle structure or metabolism leads to functional defects,  
69 such as in Duchenne syndrome[1], [2], sarcopenia[3], and cachexia[4]. Dynamic crosstalk between  
70 energetic status, muscle development, mechanical stress, and transcriptional changes is crucial to  
71 maintain muscle function. In this context, the nuclear receptor family of transcription factors (NR) is of  
72 particular interest since they are regulated by small molecules, such as metabolites and hormones[5].  
73 Although the transcriptional landscape for metabolic-functional signaling has been extensively studied  
74 in pathological and physiological conditions, a broader role of some NRs has only recently been  
75 recognized, and thus, the role of many members remains elusive[6].

76 The NRs have a modular architecture that contains a ligand-binding domain (LBD) and a zinc-finger  
77 DNA binding domain (DBD), and can be further grouped in endogenous, orphan, or adopted NRs  
78 according to the presence of an endogenous ligand, the absence of a known ligand or if a new ligand for  
79 a given NR was just identified, respectively[7]. The classical mechanistic model proposes that a small  
80 molecule binds to the LBD, changing its conformation to one of higher affinity for a transcriptional co-  
81 regulator[8], such as PGC-1 $\alpha$ , which in turn can mediate transcriptional modulation through the  
82 recruitment of histone acetylases, the mediator complex, and basal transcriptional apparatus.

83 The orphan nuclear receptor Nr2f6 (also named Ear2 or COUP-TFIII) has been characterized in a broad  
84 range of tissues, such as adipose, thyroid, liver, brain, and the immune system, where it plays different  
85 and even antagonistic roles[9]. Nr2f6 can impair adipocyte differentiation, increase cancer cell  
86 proliferation, induce both resistance and susceptibility to antitumor drugs, and promote the development

87 of fatty liver disease[10]. In ovarian cancer cells, Nr2f6 binds to the histone acetylase P300 at the  
88 Notch3 promoter, increasing histone H3 K9 and K27 acetylation to activate transcription, increasing cell  
89 proliferation and chemoresistance[11]. So far, the most extensively defined role of Nr2f6 is in the  
90 immune system, in which it directly and strongly suppresses interleukins 17, 21, 2 and interferon  $\gamma$   
91 transcription by interacting with the NFAT/AP-1 complex at the promoters of these genes[12], [13].  
92 Curiously, Nr2f6 has been reported both as a transcriptional repressor and activator, but the context that  
93 defines its activity state is unknown. Recently, Nr2f6 was classified as a stripe transcription factor[14],  
94 i.e. it can bind to low-complexity motifs together with other transcription factors in a broad range of  
95 promoters, regulating chromatin accessibility. This indicates that the function of Nr2f6 in diverse  
96 environments is influenced not only by its DNA occupancy but also by the presence and activity of  
97 other transcription factors. Whether the current understanding of the role of Nr2f6's can be applied to  
98 other tissues, such as skeletal muscle is unknown. Therefore, we sought to characterize the molecular  
99 mechanisms and functional roles of Nr2f6 in skeletal muscle biology both *in vitro* and *in vivo*. We  
100 discovered that Nr2f6 overexpression in skeletal muscle disrupts oxidative metabolism by directly  
101 repressing PGC-1 $\alpha$  and the uncoupling protein 3 (UCP3) gene expression, which impairs mitochondrial  
102 function. Moreover, Nr2f6 induces core genes of cell cycle progression and in skeletal muscle activates  
103 immune cells, increasing inflammation, reducing mass, changing fiber type, and reducing force  
104 production, collectively causing a sarcopenic-like state.

## 105 **RESULTS**

### 106 **Nr2f6 regulates muscle cell metabolism and differentiation.**

107 Genetic manipulations of Nr2f6 at the whole-body level and *in vitro* have been conducted[10], [11],  
108 [23], [24], but the role of this NR in muscle models is underexplored. We used siRNA-mediated  
109 depletion of Nr2f6 in C2C12 myocytes to verify the outcomes on the transcriptomic landscape  
110 (Supplementary Figure 1A). The 1849 differentially regulated genes, 920 upregulated and 939  
111 downregulated, could be grouped into five main classes, with increased expression of genes related to

112 muscle differentiation, contraction, and metabolism and decreased expression of genes with roles in cell  
113 cycle and DNA packaging (Figure 1A-D). In fact, among the 20 most significant altered genes, nine  
114 are linked to muscle contraction (*RYR1*, *TTN*, *MYH3*, *MYH2*, *ACNT2*, *ATP2A1*, *MYL1*, *TNNC2*,  
115 *MYOM3*) are upregulated by Nr2f6 knockdown (Figure 1A). Accordingly, a panel of canonical markers  
116 of muscle differentiation containing muscle regulatory factors (MRFs) and myosin isoforms (Figure 1E)  
117 reveals that the Nr2f6 knockdown enhanced C2C12 differentiation. Indeed, data generated in our  
118 transcriptomic analysis was correlated with a publicly available C2C12 myogenesis dataset  
119 (Supplementary Figure 1B). Consistently, the proteins coded by the upregulated genes belonged mostly  
120 to the sarcomere, contractile fiber, and cytoplasm location ontologies. Since both an increase in cellular  
121 oxidative capacity and the activation of the PI3K pathway are required for myogenesis[25], [26], we  
122 verified whether genes of the main pathways of regulation of glycolysis and fatty acid oxidation were  
123 affected and found that several energy sensors such as *AKT2*, *PRKAG3* subunit of AMPK, and mTOR  
124 complex were upregulated by Nr2f6 loss-of-function (Figure 1F). Myogenic differentiation demands the  
125 withdrawal of the cell cycle and both processes are regulated in a concerted manner[27], [28].  
126 Accordingly, the downregulated genes were related to different phases of cell division, with the  
127 enrichment of proteins related to DNA replication, packaging, and chromosome separations. Of note,  
128 essential components of the cell cycle progression such as *CDC25B/C* phosphatases and *CDK1/4* kinase  
129 promote quiescence and halt cell cycle progression in muscle progenitors when down-regulated[29]–  
130 [31]. Altogether, the changes in the myocyte's global transcriptome indicate that Nr2f6 inhibits  
131 myoblast differentiation and metabolism. Considering the differences between mouse and human  
132 myogenic cell's transcriptional landscape[32] we verified whether the result of Nr2f6 depletion in  
133 differentiation markers would be translatable to human primary human skeletal muscle cells. We found  
134 that expression of *MYH1/2/7*, muscle creatine kinase, and myosin light chain kinase 1 were upregulated  
135 in human cells (Figure 1G), indicating a conserved role for Nr2f6 as repressor of myogenesis.

136 **Increase in cell oxidative capacity by Nr2f6 knockdown.**

137 Given the enrichment of genes of oxidative metabolism, we first sought to verify the functional effects  
138 of Nr2f6 knockdown on metabolism. Oxygen consumption assays (Figure 2A), using palmitate as the  
139 major substrate for energy production, provided evidence that Nr2f6 knockdown promoted an increase  
140 in maximal respiration capacity after the addition of the uncoupler (carbonyl cyanide m-chlorophenyl  
141 hydrazone) CCCP and the spare capacity. Although there was no difference between control and  
142 knockdown respiratory parameters in high-glucose media (Supplementary Figure 2A, B), the  
143 extracellular acidification rates were reduced, without a reduction of total ATP pool, which was  
144 confirmed by lower lactate concentration in knockdown cells (Figure 2B, C, S2C). These results are  
145 supported by alterations in the expression of the pyruvate carboxylase, insulin-dependent glucose  
146 transporter, and fatty acid transporters (Figure 2D, E). Together, these results indicate Nr2f6 knockdown  
147 increases pyruvate and acetyl-CoA flux to the mitochondria, which could be reinforced by upregulation  
148 of the glucose transporter *GLUT4*, the anaplerotic enzyme pyruvate carboxylase (PC), and fatty-acid  
149 transporters. Our analysis of ENCODE chromatin immunoprecipitation-sequencing (ChIP-seq) data for  
150 Nr2f6 in K562 and HepG2 cells indicates an increase in mitochondrial genes related to lipid metabolism  
151 (Supplementary Figure 1C). We also identified significant enrichment of kinases related to the insulin  
152 signaling pathway when analyzing genes affected by Nr2f6 knockdown in the RNA-seq data and genes  
153 with Nr2f6 binding within the promoter region in ENCODE with ChIP-seq data (Supplementary Figure  
154 1C, D). Considering the increase in the efficiency of the Nr2f6 silenced myocytes to oxidize lipids, we  
155 hypothesized that depletion of Nr2f6 would be protected against lipid overload in skeletal muscle.  
156 Stable Nr2f6 knockdown in myotubes protected (50%) against palmitate-induced cell death and reduced  
157 mitochondrial superoxide production (40%) and decreased cytosolic reactive oxygen species (20%)  
158 (Figure 2F, G, H). Since Nr2f6 knockdown can increase lipid handling capacity by upregulating  
159 mitochondrial and cytosolic lipid transporters, mitochondrial proteins, and TCA cycle anaplerotic genes,  
160 thereby increasing oxygen consumption, we verified whether Nr2f6 is modulated by palmitate treatment  
161 *in vitro* and by high-fat diet *in vivo* in rodents[33], both pathophysiological conditions of increased lipid

162 oxidation and supply (Figure 2I-K, S2D, E). Our findings demonstrate that Nr2f6 expression is  
163 consistently reduced under these conditions, indicating a role as an energy stress response gene that  
164 facilitates metabolic adaptations to lipid oxidation. Collectively, the data provide evidence that Nr2f6  
165 inhibition protects against lipid overload by increasing lipid handling capacity in skeletal muscle.

### 166 **Nr2f6 directly represses PGC-1 $\alpha$ and UCP3 expression.**

167 We recently provided evidence that the transcriptional regulation of *UCP3* by the peroxisome  
168 proliferator-activated receptor  $\gamma$  co-receptor 1- $\alpha$  (PGC-1 $\alpha$ ) is essential for the maintenance of myotube  
169 viability during lipid overload, by preventing the production of reactive oxygen species (ROS) [34],  
170 [35]. Considering a similar phenotype by Nr2f6 knockdown in myotubes, we investigated whether  
171 Nr2f6 regulates the same pathway. We found that Nr2f6 overexpression reduced both *UCP3* and *PGC-*  
172 *1 $\alpha$*  mRNA in myotubes, which also translated to both reduced PGC-1 $\alpha$  protein content and expression of  
173 its mitochondrial electron transfer chain (ETC) target genes (Figure 3A-B). Using luciferase reporter  
174 assays, we observed Nr2f6 overexpression reduced PGC-1 $\alpha$  promoter activity, suggesting direct  
175 repression. Conversely, Nr2f6 knockdown in C2C12 myotubes increased PGC-1 $\alpha$  downstream ETC  
176 targets (Figure 3D). Further investigation into the regulation of *UCP3* transcription by Nr2f6 using 7kbp  
177 *UCP3* promoter reporter plasmid showed a reduction in the luciferase signal by Nr2f6 overexpression  
178 and an increase in activity following Nr2f6 knockdown (Figure 3E). We scanned the *UCP3* promoter  
179 region and found an Nr2f6 response element downstream of the transcription initiation site, which  
180 coincided with the open chromatin region and peaks of known the *UCP3* transcription factors, Myod1  
181 and Myogenin (Figure 3F), further supporting the notion that Nr2f6 directly repressed *UCP3* expression.  
182 The effects of Nr2f6 knockdown on *UCP3* and *PGC-1 $\alpha$*  expression could be reproduced in human and  
183 mouse primary myotubes (Figure 3G, S3A). *UCP3* transcription is regulated by peroxisome proliferator-  
184 activated receptors (PPARs) and estrogen-related receptors (ERRs) in skeletal muscle[36], [37],  
185 however, Nr2f6 silencing did not change the transactivation of responsive elements (Supplementary  
186 Figure 3B). Collectively, our results indicate that Nr2f6 is a bona fide transcription regulator of *UCP3*

187 and PGC-1 $\alpha$ . Given that UCP3 is a PGC-1 $\alpha$  target, these results indicate that Nr2f6 represses *UCP3*  
188 expression indirectly by downregulating *PGC-1 $\alpha$*  and by directly binding to the *UCP3* promoter region.

189 **Nr2f6 activates the cell cycle and represses the expression of genes involved in muscle contraction**  
190 **and oxidative metabolism.**

191 We next explored the effects of Nr2f6 overexpression *in vivo* by electroporation in the *tibialis anterior*  
192 muscle of mice, using the contralateral muscle as control, and studied the global transcriptomic changes  
193 by microarray. There were 3796 genes within the criteria for differential expression (FDR <0.05, Fold  
194 change >2), among which, 1915 were downregulated and 1781 were upregulated, with Nr2f6  
195 overexpression having a major effect on the hierarchical clustering (Figure 4A). Consistent with earlier  
196 reports that highlight Nr2f6 as a gatekeeper of the immune system[24], gene ontology analysis of the  
197 upregulated genes shows enrichment of biological processes and pathways related to the immune system  
198 (Figure 4B). RT-qPCR was used to validate markers modulated in microarray analysis. We found that  
199 indicators of lymphocyte activation *CD44*, the marker for macrophage/monocyte activation *CD68*, and  
200 the macrophage marker *F4-80* were upregulated in Nr2f6 expressing muscle (Figure 4E). Accordingly,  
201 *TGF $\beta$* , a potent inhibitor of hematopoietic cell activation, and the marker for endothelial and non-  
202 differentiated hematopoietic cells were downregulated, consistent with an increase in the number and  
203 activity of immune system-derived cells, indicating that Nr2f6 might activate resident cells of the  
204 immune system and/or promote the invasion of circulating cells. Nr2f6 overexpression also increased  
205 expression of Myogenin and, to a lesser extent, *MYOD*, however the downstream targets genes myosin  
206 heavy chains 1 and 2 decreased (Figure 4D). Downregulated genes were enriched in energetic  
207 metabolism pathways, mitochondria, and muscle contraction terms (Figure 4C), reinforcing the  
208 functional phenotypes described *in vitro*. Importantly, the hereby proposed Nr2f6 targets, namely *UCP3*  
209 and *PGC-1 $\alpha$* , were downregulated by Nr2f6 overexpression (Figure 4F). The lipid transporters *CD36*  
210 and *CPT1B*, as well as subunits of the respiratory chain complexes, which were upregulated by Nr2f6  
211 knockdown *in vitro*, were also downregulated by Nr2f6 overexpression. Additionally, the expression of

212 reactive oxygen species scavengers *SOD1*, *SOD2*, and catalase genes was decreased (Figure 4F).  
213 Collectively, these findings support our functional results and indicate mitochondrial function was  
214 impaired by Nr2f6 overexpression.

### 215 **Nr2f6 inhibits muscle development and contraction.**

216 Since Nr2f6 overexpression negatively affects the mRNA expression of genes involved in muscle  
217 contraction and development, we next investigated whether the Nr2f6 gain-of-function would impair  
218 muscle morphology and function by performing immunostaining for myosin heavy chain (MHC)  
219 isoforms and *ex vivo* contraction experiments, respectively. Intriguingly, Nr2f6 overexpressing *tibialis*  
220 *anterior* (TA) weighted less and were visually paler compared with control muscle (Figure 5A).  
221 Consistent with these observations, Nr2f6 overexpression reduced the total number of fibers (21%),  
222 which together with the increase in cell death-related genes (Figure 4B), and the increase in the  
223 atrogenes cathepsin and calpain 2[38] (Supplementary Figure 4A), characterizes a state of atrophy  
224 (Figure 5B, C). Stratification by fiber type showed that this reduction is particularly due to the decrease  
225 in type IIB fibers, which were reduced by 23%, and although there was a tendency to decrease IIX fiber  
226 number (Figure 5D), there was no statistical significance in these comparisons or the number of IIA  
227 fibers. We then overexpressed Nr2f6 in the *flexor digitorum brevis* (FDB) and performed *ex vivo*  
228 contractions to verify alterations in muscle force production and fatigability. Consistent with the  
229 immunostaining data, mass-corrected maximal force production was reduced (60%) (Figure 5E), but  
230 time to fatigue was unaltered in Nr2f6 overexpressing muscles (Supplementary Figure 4B). Since the *ex*  
231 *vivo* contraction assay surpasses the neuromuscular system by direct electric stimulation, disregarding  
232 action potential issues, fatigability is mostly induced by detriments in calcium homeostasis, such as  
233 reduced Ca<sup>2+</sup> sensitivity, sarcoplasmic Ca<sup>2+</sup> reuptake, and release[39]. Therefore, we cannot exclude the  
234 possibility that the time to fatigue is also affected *in vivo* in Nr2f6 gain-of-function models. So far, these  
235 findings strongly suggest induction of atrophy, worsened by an inflammatory state and an imbalance  
236 between satellite cell proliferation and differentiation.

## 237 **Nr2f6 modulates myoblasts' proliferation rates.**

238 Next, we investigated whether Nr2f6 regulates cell cycle genes and myoblast proliferation. Thus, we  
239 compared differentially expressed genes identified in the microarray of the Nr2f6 overexpression in TA  
240 muscle with the RNA-seq transcriptomics from C2C12 myocytes after transient Nr2f6 knockdown. We  
241 found 706 genes were differentially expressed in both experiments, whereby 446 genes were modulated  
242 in opposite directions indicating a direct regulation by Nr2f6 or a conserved effect of Nr2f6 modulation  
243 in both models (Figure 6A). We further scanned the promoter regions of these genes consisting of 3 kbp  
244 upstream and downstream of the transcription start site, for the Nr2f6 binding motif. We found 206  
245 matches in unique genes, whereby 73 were upregulated and 133 downregulated by Nr2f6  
246 overexpression. The interaction network of these high-confidence targets (Figure 6B) reveals that the  
247 most connected genes are upregulated by Nr2f6 overexpression and are mostly related to the cell cycle,  
248 which emphasizes the role of Nr2f6 as a promoter of cell division, and further reinforces the dysplastic  
249 phenotype observed in the gain-of-function experiments *in vivo*. Investigation of canonical pathways of  
250 myogenesis cell proliferation and stemness in Nr2f6 overexpressing TAs (Figure 6C, D) showed that the  
251 content of the proliferating cell nuclear antigen (PCNA), an important general marker for cell  
252 proliferation[40], was increased by Nr2f6 overexpression. Together with the increase of the muscle-  
253 specific satellite cell marker Pax7, and the activation by phosphorylation of the stemness markers  
254 GSK3a/b[1], [41], ERK[42], [43], and S6, these results point to an increase in myogenic progenitors and  
255 the infiltration of other cell types, such as cells of the immune system. Nr2f6 overexpression and  
256 knockdown can promote or inhibit cell proliferation in cancer cells, respectively[44]–[46]. Our doubling  
257 time experiments (Figure 6E, G) confirm this effect is also conserved in C2C12 myoblasts, with an  
258 increase of 4 hours in the average doubling time in knockdown cells and a decrease of 3.5 hours in  
259 Nr2f6 overexpression stable cell lines. Moreover, RT-qPCR validation of major markers of cell cycle  
260 progression inhibitors *RBI* and *P21* show an increase in both genes by Nr2f6 knockdown and a  
261 tendency towards downregulation of *RBI* by Nr2f6 overexpression (Figure 6F, H). Collectively, these

262 results indicate that the function Nr2f6 function as an important repressor of cell cycle progression is  
263 conserved in muscle models.

## 264 **DISCUSSION**

265 Numerous nuclear receptors are necessary for the maintenance of muscle mass[47], [48]. For example,  
266 whole-body knockout of Nr1d1 (Rev-ERB $\alpha$ , Ear-1) leads to an increase in atrophic genes, a decrease in  
267 muscle mass, and a relative increase in low-diameter fibers[49]. More broadly, muscle-specific  
268 knockout of the nuclear receptor co-repressor 1 (NCoR1) leads to skeletal muscle hypertrophy and  
269 increased oxidative metabolism[50]. Here, we found evidence that a disruption in myogenesis also  
270 follows Nr2f6 overexpression *in vivo* and *in vitro*, and myoblast proliferation rates are increased.  
271 Remarkably, Nr2f2 (COUP-TFII), an Nr2f6 interactor, is among the few nuclear receptors found to  
272 promote muscle wasting[51], [52]. However, Nr2f2 expression in myogenic progenitors impairs muscle  
273 differentiation in mice by directly repressing genes related to myoblast fusion and proliferation[53],  
274 [54], implying that myogenesis is disrupted in a different stage. Future studies should address the  
275 redundancy of these NRs in muscle function.

276 Most of the transgenic and knockdown models provide evidence to suggest that nuclear receptors are  
277 involved in a general activation of oxidative metabolism[47]. For example, the muscle-specific Nr4a3  
278 transgenic mouse displays a marked increase in mitochondrial density and fast-to-slow fiber switch[55].  
279 This general rule is reinforced by the fact that mice lacking nuclear receptor co-activators, such as PGC-  
280 1 $\alpha$  and MED1[56], or overexpressing the co-repressor RIP140[57], have decreased mitochondrial  
281 density and fewer oxidative fibers. Conversely, here we show that Nr2f6 is an exception to this model in  
282 skeletal muscle since this nuclear receptor can directly reduce PGC-1 $\alpha$  and UCP3 promoter activity,  
283 thereby increasing the susceptibility of muscle cells to lipid overload by reducing fatty-acid oxidation  
284 and increasing reactive oxygen species production. Transgenic mouse models overexpressing UCP3 in  
285 muscle are consistently reported to have improved glucose homeostasis under chow and high-fat diet  
286 (HFD) conditions, as well as resistance to obesity-induced diabetes[58]–[60]. Moreover, increased

287 levels of circulating lipids increase UCP3 expression[61], [62]. Here, we demonstrate that direct fatty-  
288 acid exposure in C2C12 myotubes or conditions of increased  $\beta$ -oxidation *in vivo* reduces Nr2f6 mRNA  
289 expression and protein content, further reinforcing the finding that Nr2f6 mediates the positive effects of  
290 UCP3 under physiological conditions. Importantly, we show that the regulation of *UCP3* and *PGC-1 $\alpha$*   
291 expression by Nr2f6 is conserved in human skeletal muscle cells.

292 Sarcopenia is the age-related loss of muscle mass and function, with the reduction of the number and  
293 size of myofibers, a switch from type II to I fibers[63], and an underlying mitochondrial  
294 dysfunction[64]. This phenotype is closely reproduced by Nr2f6 overexpression in skeletal muscle. In  
295 contrast to most members of the NR family, Nr2f6 overexpression not only induces a sarcopenic-like  
296 phenotype, with loss of muscle mass and inflammation but also reduces muscle strength and affects  
297 energy metabolism. Interestingly, Nr2f6 is upregulated 2-fold in skeletal muscle hereditary spastic  
298 paraplegia[65], a disease characterized by progressive lower limb muscle weakness, sometimes  
299 accompanied by mitochondrial dysfunction and morphological fiber defects[66], [67]. While additional  
300 experiments are warranted to assess the effects of Nr2f6 ablation *in vivo*, Nr2f6 knockdown in myotubes  
301 increases myosin heavy chain expression and improves mitochondrial function, suggesting that  
302 inhibition of Nr2f6 might be efficacious in the treatment of sarcopenia or other myopathies. Nr2f6  
303 agonists have been proposed as a possible treatment for colitis[68], but based on our finding that Nr2f6  
304 gain-of-function alone provokes muscle loss, the use of such agonists should be further evaluated for the  
305 treatment of patients suffering from myopathies and cachexia. Considering the known effects of Nr2f6  
306 in the inflammatory response, the atrophic phenotype may be supported by a role of Nr2f6 in immune  
307 cells. Nonetheless, the antagonistic transcriptional changes induced by Nr2f6 overexpression *in vivo*,  
308 and knockdown *in vitro* strongly indicate a direct action of Nr2f6 in the myofibers as the major driver of  
309 the functional changes.

310 A conceivable model elucidating the mechanism by which Nr2f6 overexpression culminates in a  
311 reduction of muscle force production (Figure 7), entails the downregulation of genes engaged in various

312 facets of muscle contraction, such as muscle structure, calcium cycling, and action potential. Notably, a  
313 few of these genes constitute high-confidence targets. The ryanodine receptor 1 (*RYR1*) is a major  
314 component of the calcium release complex, which permits calcium efflux from the sarcoplasmic  
315 reticulum into the cytosol. As such, *in vivo* knockdown and mutations of *RYR1* can cause severe  
316 myopathies[69]. Other putative targets including myosin light chain kinase 4 (*MYLK4*) and myomesin 1  
317 (*MYOM1*) are downstream of the androgen receptor (AR), which mediates the effects on muscle force  
318 production[70]. Interestingly, we found that the spermine oxidase gene (*SMOX*), another important  
319 target of the AR in muscle[71], [72] is downregulated by Nr2f6 overexpression *in vivo*, upregulated by  
320 Nr2f6 silencing in C2C12 myocytes, and contains Nr2f6 binding motifs at the promoter region. The  
321 direct link between Nr2f6 and the spermine synthesis pathway and a possible interaction with the AR  
322 warrant further studies.

323 Targeted studies provided evidence that Nr2f6 activates gene expression by tethering to the promoters of  
324 *circRHOT1*[73], *DDAI1*[74], and *CD36*[10], and represses the expression of numerous others such as  
325 *IL17*, *IL21*, Renin, and Oxytocin[44], [45], [75], [76]. More broadly, our transcriptomics experiments  
326 display an equilibrated number of genes up- and downregulated, further implying that Nr2f6 is a dual-  
327 function transcription factor. Interestingly, Nr2f6 is a target of MiR-142-3p[77], raising the possibility  
328 that miRNAs, besides protein partners and post-translational modifications[44], might aid in the  
329 regulation of Nr2f6 activity. Further studies should help to elucidate the mechanism by which Nr2f6 acts  
330 as a repressor or activator of gene expression. The case of *CD36* illustrates context-dependent regulation  
331 given that this gene is activated in the liver[10], but repressed in skeletal muscle by Nr2f6 in mice and  
332 humans. This finding suggests that Nr2f6 may be bound to DNA but kept in a repressive state by post-  
333 translational modifications or interaction partners, such as RAR Related Orphan Receptor  $\gamma$  (*ROR $\gamma$* ),  
334 another regulator of *CD36* transcription in muscle[78] and liver[79]. In Th17 lymphocytes, Nr2f6 can  
335 compete with *ROR $\gamma$*  for binding at the *IL17* promoter, maintaining the repressive state. This relationship  
336 may also be present in skeletal muscle.

337 As reported for other cell types[11], Nr2f6 also modulates myoblast proliferation *in vitro* and increases  
338 the expression of proliferation markers such as *PCNA* and *KI67 in vivo*. In Nr2f6 overexpressing  
339 muscle, Myogenin expression is also increased. However, the myosin heavy chains and other indicators  
340 of terminally differentiated myofibers are sharply reduced. These findings raise the possibility that the  
341 Nr2f6-overexpressing myoblasts proliferate but fail to assemble into robust myofibrils due to a  
342 dysregulated temporal modulation of the MRFs during myogenesis, which critically impairs muscle  
343 fiber formation and force production. Key regulators of cell cycle cyclin B1 and Cdk1 are placed among  
344 high-confidence direct targets of Nr2f6. Cyclin B1 interacts with Cdk1 and is necessary for kinase  
345 activity[80] and progression through the G2 mitotic phase. Moreover, Ccnb1 overexpression is  
346 increased in several cancer types and ectopic expression increases cell proliferation rates [81], [82]. The  
347 simultaneous effect of Nr2f6 modulation on cell cycle and differentiation markers might also be  
348 sustained indirectly by the expression of the retinoblastoma protein, which is responsible for cell cycle  
349 arrest through the inhibition of the E2F family of transcription factors. In a feedback loop, E2F TFs  
350 antagonize MyoD1, which induces Rb expression, thereby linking processes of proliferation and  
351 differentiation[83], [84].

352 Our findings provide evidence that Nr2f6 plays a critical role in the regulation of several aspects of  
353 muscle biology. Nr2f6 modulation alone can determine myoblast proliferation rates, consolidating its  
354 role as a major regulator of cell cycle progression. In summary, we report that Nr2f6 is a novel regulator  
355 of muscle contraction and metabolism, which may hold promise as a possible strategy for the treatment  
356 of muscle wasting and metabolic diseases.

## 357 **MATERIALS AND METHODS**

358 The main reagents, tools, and models necessary for replicating the reported results are listed in  
359 Supplementary Table 2.

360 **Cell culture** Human primary skeletal muscle cells were isolated from healthy female and male donors  
361 (Al-Khalili et al. 2004), age  $55 \pm 5$  years old, BMI  $25.6 \pm 1.5$  kg.m<sup>-2</sup>. Myoblasts were maintained in

362 Growth Media (DMEM/F12 High Glucose (Gibco, #31331093) supplemented with 10 mM HEPES  
363 (Gibco #15630-056), 16% Fetal calf serum (Sigma, #F7524), and antibiotics (Gibco #15240-062) and  
364 differentiated at the confluence with fusion media (74% DMEM High Glucose (Gibco, 31966-021),  
365 20% 199 Medium (Gibco #31150-022), 20 mM HEPES, antibiotics, 0.03 µg/mL Zinc Sulfate (Sigma  
366 #Z4750), 1.4 mg/mL Vitamin B12 (Sigma #V6629), and 2% Fetal Calf Serum) supplemented with  
367 100ug/mL Apotransferrin (Biotechnne #3188-AT-001G) and 1.7 mM Insulin (Actrapid Penfill, Novo  
368 Nordisk #13509) before use. After 5 days of fusion, apo transferrin and insulin were removed from the  
369 media, and cells were incubated for 4 more days. Cells were cultivated in a humidified atmosphere  
370 containing 7.5% CO<sub>2</sub> and regularly tested for mycoplasma. C2C12s, MEFs, and HEK cells were  
371 maintained in DMEM High Glucose (Gibco, 31966-021) supplemented with 4 mM L-glutamine, 10%  
372 fetal bovine serum, 1 mM sodium pyruvate, and antibiotics. Fetal bovine serum was substituted by 2%  
373 horse serum to induce myogenesis in C2C12 cells when 90-100% confluence was reached, and  
374 experiments were performed 5 days later.

375 **Primary mouse skeletal muscle cells** Mice's primary skeletal muscle cells were isolated from wild-type  
376 C57Bl6/JUnib as described (Araujo et al. 2020). After euthanasia, hindlimb muscles were dissected and  
377 digested with collagenase II, trypsin, and DNase I. Cells were sifted through a 70 µm cell strainer and  
378 plated in 0.1% Matrigel-coated plates. Myoblasts were maintained for 2 days in DMEM High Glucose  
379 supplemented with 2 mM L-glutamine, 10% fetal bovine serum, 10% horse serum, 1 mM sodium  
380 pyruvate, and antibiotics. Myogenesis was induced by removing fetal bovine serum from the media  
381 when confluence was reached, and cells were cultivated for 5 more days. The experiments were  
382 approved by the Ethics Committee on Animal Use (CEUA/Unicamp #5626-1/2020).

383 **Animals** All electroporation experiments were conducted following the guidelines of animal welfare  
384 and were approved by the Stockholm North Animal Ethical Committee (Stockholm, Sweden). Male  
385 C57Bl6/J mice were acquired from Jackson Labs and maintained at 12/12h light/dark cycle under  
386 controlled temperature and humidity, and *ad libitum* access to food (Specialized Research Diets, #

387 801722) and water. The use of animals for high-fat diet experiments was approved by the Ethics  
388 Committee on Animal Use (CEUA/Unicamp #5626-1/2020) and all the welfare guidelines of the  
389 National Council of Control of Animal Experimentation (CONCEA) were followed. Male  
390 C57Bl6/JUnib mice were kept under the same conditions described above. Mice were provided a high-  
391 fat diet (PragSolucoes #0015, 60% kcal from lipids) at 4 weeks of age for 16 weeks; littermates were fed  
392 a standard chow diet as a control.

393 **Reactive oxygen species measurement** Cells were incubated with 5 nM MitoSOX (Invitrogen,  
394 #M36008) or 5  $\mu$ M Dihydroethidium (DHE, Invitrogen, #D11347) in DMEM without phenol red  
395 supplemented with 1 mM Sodium Pyruvate, 4 mM L-glutamine, and 25 mM Glucose for 30 min and  
396 washed three times before reading in a plate reader 510/580 nm (ex/em) or 520/610 nm (ex/em) for  
397 DHE. Samples were fixed and stained with Crystal Violet for normalization.

398 **RT-qPCR** Total RNA was extracted from cells with TRIzol (Invitrogen #15596-018) following the  
399 manufacturer's instruction and cDNA was synthesized with a High-Capacity Reverse Transcription kit  
400 (Applied Biosystems #4368814). cDNA was diluted to 10 ng/ $\mu$ L and 20 ng was used for qPCR  
401 reactions. NormFinder (Andersen, Jensen, and Ørntoft 2004) was used to decide the best combination of  
402 internal controls among RPL39, PPIA, HPRT, 18S, ACTB, and GAPDH. In the *in vivo* electroporation  
403 experiments, gene expression was normalized using HPRT-PPIA geomean with TaqMan probes or  
404 HPRT-RPL39 geomean when SYBER green was used. For other experiments, gene expression was  
405 normalized with multiplexed HPRT when TaqMan probes were used or with RPL39 when SYBER was  
406 used. Relative expression was calculated by the  $\Delta\Delta C_T$  method (Livak and Schmittgen 2001) and is  
407 expressed as fold change over the indicated control. The primers and probes used are listed in  
408 Supplementary Table 1.

409 **RNA-seq** Total RNA was extracted with TRIzol and the upper phase containing RNA was loaded into  
410 RNeasy columns (Qiagen, #74004) after the addition of isopropanol, following the manufacturer's  
411 instructions. cDNA libraries were prepared with TruSeq Illumina Total RNA Stranded (Illumina) with

412 Ribo-zero rRNA depletion (Illumina). Sequencing was outsourced to Macrogen Inc. (Seoul, South  
413 Korea) and performed in a HiSeq X (Illumina), producing an average of 50.8 Mreads, 95% above Q30.  
414 Sequence trimming and adapter removal were done with Trimmomatic (Bolger, Lohse, and Usadel  
415 2014) with the following modifications: HEADCROP = 10, MINLEN = 20, AVGQUAL = 20.  
416 Reminiscent reads were aligned to the mouse genome (Ensembl GrCm38) with RNA Star 2.7.2b and  
417 gene-level counts were calculated with featureCounts v1.6.4. Differential expression was performed  
418 with EdgeR with TMM normalization and p-value adjustment using Benjamini and Hochberg  
419 normalization with a 0.05 false discovery rate (FDR) cut-off. The Galaxy platform was used to process  
420 all data. Pathway enrichment analysis was done in g:Profiler with an FDR cutoff of 0.01. Interaction  
421 networks were generated by String.db and analyzed with CytoScape v3.8 using the EnrichmentMap  
422 plugin.

423 **Palmitate treatment** Palmitate (Sigma, #P5585) in absolute ethanol was conjugated with 1% fatty-acid-  
424 free bovine serum albumin (Sigma, #A7030) in cell media for 15 min at 55 °C to a 500 µM final  
425 concentration. Cells were treated with fresh solutions of palmitate or vehicle (1%BSA, 1% ethanol) for  
426 20 hours.

427 **Promoter transactivation assays** Luciferase reporter assays were performed in MEF cells transfected  
428 with a UCP3 reporter plasmid (Harmancey et al. 2015) (UCP3 EP1, Addgene #71743) or PGC-1α 2kb  
429 promoter (Handschin et al. 2003) (Addgene #8887), normalization plasmid coding for *Renilla* luciferase  
430 (pRL-SV40) and either control empty vector or Nr2f6 coding plasmid (Gift from Dr. Gottfried Baier,  
431 Medical University of Innsbruck, Austria) using Lipofectamine 3000. Luciferase activity was measured  
432 with DualGlo Luciferase Reporter Assay (Promega, #E2920). For knockdown assays, cells were  
433 transfected with siRNAs one day before the transfection of the reporter plasmids.

434 **siRNA knockdown** C2C12 cells were transfected with 200 nM non-target siRNA (siScr, Qiagen) or  
435 siNr2f6 (Sigma) using Lipofectamine RNAiMax (Invitrogen) following manufacturer's instructions  
436 concomitantly with the myogenesis media switch. Experiments were performed on the third or fiftieth

437 day of differentiation. Primary human skeletal muscle cells were transfected at the fiftieth day of  
438 differentiation with 5 nM siScr (Ambion) or siNr2f6 (Ambion).

439 **Stable cell lines** The Nr2f6-myc insert was subcloned from the Nr2f6-myc-flag plasmid into the  
440 pBABE-Puro vector using standard PCR with primers spanning the transcription start site and the myc  
441 tag. The viral particles for generating the overexpression HEK293T cells were transfected with pCMV-  
442 VSVG, pCL-Eco, and the pBABE-Nr2f6-myc or empty vector. For producing viral particles with the  
443 knockdown plasmid, HEK293T cells were transfected with packaging vectors pCMV-dR8.2 dvpr,  
444 pCMV-VSVG, and pLKO.1-shGFP or shNr2f6 (TRCN0000026147). Cell medium containing virions  
445 was collected, filtered at 0.45  $\mu\text{m}$ , and stored at  $-80\text{ }^{\circ}\text{C}$  until further use. Virus concentrations were  
446 titrated by the minimal dilution method, C2C12 cells were transduced with 1 MOI, and cells were  
447 selected with 2  $\mu\text{g}/\text{mL}$  puromycin for 4 days. The clonal selection was performed in the knockdown  
448 cells and the clones were validated as indicated. The modified cells and their respective controls were  
449 cultivated synchronously under the same conditions.

450 **Electroporation** Mice were kept under 2% isoflurane-induced anesthesia and the *tibialis anterior*  
451 muscles were injected with 30  $\mu\text{L}$  of 1 mg/mL hyaluronidase (Sigma, #H3506). After 2 hours, the lateral  
452 and contralateral *tibialis anterior* were injected with 30  $\mu\text{g}$  of either control empty vector pCMV6 or  
453 Nr2f6-myc-flag overexpression plasmid (Origene, #MR206083) and 220V/cm were applied in 8 pulses  
454 of 20/200 ms on/off (ECM 830 Electroporator, BTX). Terminal experiments were performed 9 days  
455 after electroporation with 13 weeks old mice. For electroporation of FDB muscles, after anesthesia 10  
456  $\mu\text{L}$  of 1 mg/mL hyaluronidase were injected into the footpads and after 1 hour, 20  $\mu\text{g}$  of the control or  
457 Nr2f6 coding plasmids. Mice rested for 15 minutes and then 75V/cm were applied in 20 pulses of 20/99  
458 ms on/off with the aid of sterile gold acupuncture needles.

459 **Contraction** Mouse FDB muscles were electroporated as described and dissected 8 days later. With the  
460 muscles still attached to the tendons, contraction threads were tied at the most distal and proximal  
461 tendons, and the muscles were transferred to contraction chambers containing prewarmed and

462 continuously oxygenated KHB buffer at 30°C. The optimal muscle length was determined, and all  
463 subsequent measurements were performed at this length. For maximal force production mice, FDBs  
464 were stimulated at 10, 30, 50, 80, 100, and 120 Hz for 1 second and with 0.1 ms pulses. Muscles were  
465 left to rest for 5 minutes before starting the fatigue protocol as follows: 0.1 s train duration, 0.3 s train  
466 delay, and pulses of 0.1 ms at 50 Hz. The maximal force was evaluated again 5 min after the end of the  
467 fatigue protocol to check muscle integrity. Muscles were weighed and protein extraction was performed  
468 to normalize. The maximal force was calculated with the difference of the peak force at 120 Hz and the  
469 baseline and time to fatigue taken as the time necessary to reach 50% intensity of the first peak.

470 **MHC Staining** Electroporated *tibialis anterior* muscles were embedded in O.C.T, immediately frozen  
471 in nitrogen-cooled isopentane, and stored at -80°C until cryosectioning. Muscle slices were blocked (5%  
472 Goat serum, 2% BSA, 0,1% sodium azide in PBS) for 3 hours at room temperature and probed with  
473 primary antibodies overnight at 4°C in a humidified chamber. The slides were washed 3 times with PBS  
474 and incubated with Alexa Fluor conjugated secondary antibodies for 2 hours at room temperature.  
475 Coverslips were mounted with ProLong antifade Diamond and whole sections were imaged with a  
476 fluorescent scanning microscope at 20x magnification.

477 **Oxygen consumption assays** Oxygen consumption rates (OCR) were measured in a Seahorse XF24  
478 extracellular flux analyzer according to the manufacturer's instructions. The following drugs were used  
479 in the assay: 1 µM oligomycin (Oligo), 2 µM carbonyl cyanate m-chlorophenyl hydrazone (CCCP), and  
480 1 µM rotenone/antimycin (Rot./Ant). ATP-linked OCR was calculated by subtracting OCR post  
481 oligomycin addition from the OCR measured before. Reserve capacity was determined by subtracting  
482 basal from maximal OCR. Non-mitochondrial values were subtracted before all calculations. For fatty-  
483 acid oxidation assays, cell media was switched to low glucose 12 hours before the measurements, and  
484 cells were equilibrated in KHB supplemented with 1g/L glucose, 4 mM L-glutamine, and 1 mM sodium  
485 pyruvate for 1 hour. Immediately before the assay, BSA-conjugated palmitate was added to a final  
486 concentration of 200 µM, and the drugs were added in the same manner. During routine oxygen

487 consumption assays, cells were maintained in phenol red-free DMEM, supplemented with 4.5g/L  
488 glucose, 4 mM L-glutamine, and 1 mM sodium pyruvate, without sodium bicarbonate.

489 **Lactate measurement** Cells were grown in 96 well plates and then incubated for 3 h with 50  $\mu$ L Krebs-  
490 Henseleit Buffer (1.2 mM Na<sub>2</sub>HPO<sub>4</sub>, 2 mM MgSO<sub>4</sub>, 4.7 mM KCl, 111 mM NaCl, pH 7.3)  
491 supplemented with 25 mM glucose, 1 mM pyruvate, and 4 mM Glutamine. Lactate production was  
492 enzymatically quantified as NADH fluorescence (360 nm/460 nm) by the reverse reaction of L-lactate  
493 dehydrogenase (Rabbit muscle, L25005KU, Sigma) in a reaction containing 20  $\mu$ L cell media, 2  $\mu$ g  
494 enzyme, 50 mM Tris, and 625 mM Hydrazine in PBS. Following the assay, the cells were fixed and  
495 stained with crystal violet for cell number normalization.

496 **Western blot** Protein extracts from cells and tissues were obtained with RIPA Buffer (Thermo  
497 Scientific, # 89900) and 30  $\mu$ g loaded into SDS-PAGE gels. Proteins were then transferred to 0.45  $\mu$ m  
498 PVDF membranes, probed with the indicated primary antibodies, and detected with ECL. Band  
499 intensities were normalized by Ponceau S intensity and data is shown as fold-change over control.

500 **Microarray** RNA was extracted with TRIzol and subsequently column-purified using RNeasy Mini Kit  
501 (Qiagen). Sample integrity was assessed, and the library was prepared using Affymetrix Whole  
502 Transcript (WT) Assay kit probed in CGAS cartridge for Clariom S (mouse) following manufacturer's  
503 instructions. Total RNA quality was assessed by Agilent Technologies 2200 TapeStation and  
504 concentrations were measured by NanoDrop ND-1000 Spectrophotometer. Total RNA (150 ng) was  
505 used to generate amplified sense strand cDNA targets using GeneChip® WT Plus Reagent Kit  
506 (ThermoFisher Scientific) followed by fragmentation and labeling. 2.3  $\mu$ g of ss cDNA target was  
507 hybridized to Clariom™ S Mouse Arrays for 16 hours at 45°C under rotation in Affymetrix Gene Chip  
508 Hybridization Oven 645 (ThermoFisher Scientific). Washing and staining were carried out on  
509 Affymetrix GeneChip® Fluidics Station 450 (ThermoFisher Scientific), according to the manufacturer's  
510 protocol. The fluorescent intensities were determined with Affymetrix GeneChip Scanner 3000 7G  
511 (ThermoFisher Scientific). Transcriptome Analysis Console (TAC) software (v4.0.3, ThermoFisher

512 Scientific) was used for the analysis of microarray data. Signal values were log<sub>2</sub>-transformed, and  
513 quantile normalized using the Signal Space Transformation (SST-RMA) method. Paired comparisons of  
514 gene expression levels between sample groups were performed using moderated t-test as implemented  
515 in BioConductor package limma. Gene ontology enrichment tests were performed with g:profiler  
516 excluding electronic annotations.

517 **Cell-death assays** Cell-death assays were performed as described (Lima and Silveira 2018), with slight  
518 modifications. Propidium iodide was added to a concentration of 5 µg/mL in cell culture media and  
519 incubated for 20 minutes. Hoechst 33342 was then added to a final concentration of 1 µg/mL and  
520 samples were incubated for another 10 minutes. Fluorescence was measured at 530/620 nm (ex./em.)  
521 and 350/460 (ex./em.) nm in a plate reader.

522 **Cell doubling time** Cells (10<sup>4</sup>) were plated in four replicates in 12-well plates. Thereafter, cells were  
523 collected every 24 hours using trypsin and counted in a Neubauer chamber. The normalized data of  
524 three independent experiments were used to obtain the doubling-time regression curve with the initial  
525 number constraint.

526 **ATP measurement** Cells were grown in opaque 96-well white plates and then processed according to  
527 the manufacturer's instructions of the CellTiter-Glo® Luminescent Cell Viability Assay kit (Promega).  
528 The standard curve of ATP was determined in parallel for absolute quantitation.

529 **Bioinformatic analysis of public datasets** Nr2f6 ChIP-seq bigwig files from the ENCODE project  
530 (GSM2797593 and GSM2534343) available on GEO were used. Using the Galaxy platform, the  
531 anchoring position matrix was generated using the compute matrix command from the deeptools  
532 package, relative to human genome annotations extracted from the UCSC Genome Browser in bed  
533 format. The heatmap was obtained using the ploheatmap tool, also from the deeptools package.  
534 Pathway enrichment was analyzed using the g.profiler program (<https://biit.cs.ut.ee/gprofiler/gost>), with  
535 a significance threshold of 0.01 using the g:SCS parameter, without considering electronic term  
536 annotations. The correlation in Supplementary Figure 1B was produced with fold-changes of

537 differentially expressed genes from RNA-seq (FDR <0.05) and fold-change values (expression in  
538 myotube/expression in myoblast) from the C2C12 cell differentiation array (GSE4694) considering a p-  
539 value cut-off of 0.01, according to GEO2R. UCP3 genome locus in Figure 3E was extracted from the  
540 UCSC genome browser with the ChIP-seq tracks of Myogenin (wgEncodeEM002136,  
541 wgEncodeEM002132), MyoD (wgEncodeEM002127, wgEncodeEM002129), H3K4me  
542 (wgEncodeEM001450), H3K27Ac (wgEncodeEM001450) and DNA hypersensitivity track  
543 (wgEncodeEM003399) over NCBI37/mm9 mouse genome assembly.

544

#### 545 **Statistical analysis and quantification**

546 GraphPad Prism v7.0 was used for plotting the data and for statistical analysis. Cell culture experiments  
547 were performed independently several times with 3-4 technical replicates. Ratio paired comparison  
548 using Student's t-test was used for the analysis of human cells and electroporation experiments,  
549 otherwise, an unpaired comparison was chosen, and in both cases, a 0.05 p-value cutoff was used.  
550 Details for microarray and RNA-seq statistics are described in their respective methods section and  
551 further statistical details are presented in figure labels.

#### 552 **Acknowledgments**

553 We would like to appreciate the technical support of Ann-Marie Petterson.

#### 554 **DECLARATIONS**

#### 555 **Ethics approval and consent to participate**

556 All animal experiments were approved by the local regulatory entities, either the Stockholm North  
557 Animal Ethical Committee or by the Ethics Committee on Animal Use (CEUA/Unicamp #5626-  
558 1/2020), observing the welfare guidelines of the National Council of Control of Animal Experimentation  
559 (CONCEA). Consent to participate not applicable.

#### 560 **Consent for publication**

561 Not applicable.

562 **Availability of data and materials**

563 The materials originally produced in this study are available upon request to the lead contact. The  
564 transcriptomic data generated in this study can be accessed at the GEO (GSE229102 and GSE228202).

565 **Competing interests**

566 The authors declare no competing interests

567

568

569 **REFERENCES**

- 570 [1] Z. Ma, Z. Zhong, Z. Zheng, X. M. Shi, and W. Zhang, “Inhibition of glycogen synthase kinase-  
571  $3\beta$  attenuates glucocorticoid-induced suppression of myogenic differentiation in vitro,” *PLoS One*,  
572 2014, doi: 10.1371/journal.pone.0105528.
- 573 [2] D. Duan, N. Goemans, S. Takeda, E. Mercuri, and A. Aartsma-Rus, “Duchenne muscular  
574 dystrophy,” *Nature Reviews Disease Primers*. 2021. doi: 10.1038/s41572-021-00248-3.
- 575 [3] P. M. Coen, R. V. Musci, J. M. Hinkley, and B. F. Miller, “Mitochondria as a target for  
576 mitigating sarcopenia,” *Frontiers in Physiology*. 2019. doi: 10.3389/fphys.2018.01883.
- 577 [4] J. L. Brown *et al.*, “Mitochondrial degeneration precedes the development of muscle atrophy in  
578 progression of cancer cachexia in tumour-bearing mice,” *J. Cachexia. Sarcopenia Muscle*, 2017, doi:  
579 10.1002/jcsm.12232.
- 580 [5] K. De Bosscher, S. J. Desmet, D. Clarisse, E. Estébanez-Perpiña, and L. Brunsveld, “Nuclear  
581 receptor crosstalk — defining the mechanisms for therapeutic innovation,” *Nature Reviews*  
582 *Endocrinology*. 2020. doi: 10.1038/s41574-020-0349-5.
- 583 [6] and V. A. N. Kumar, Ashok, “Nuclear receptors as potential therapeutic targets in peripheral  
584 arterial disease and related myopathy,” *FEBS J.*, 2022, doi: 10.1111/febs.16593.
- 585 [7] M. Robinson-Rechavi, H. E. Garcia, and V. Laudet, “The nuclear receptor superfamily,”  
586 *Journal of Cell Science*. 2003. doi: 10.1242/jcs.00247.
- 587 [8] K. W. Nettles and G. L. Greene, “Ligand control of coregulator recruitment to nuclear  
588 receptors,” *Annual Review of Physiology*. 2005. doi: 10.1146/annurev.physiol.66.032802.154710.
- 589 [9] V. Klepsch, K. Siegmund, and G. Baier, “Emerging next-generation target for cancer  
590 immunotherapy research: The orphan nuclear receptor NR2F6,” *Cancers*. 2021. doi:  
591 10.3390/cancers13112600.
- 592 [10] B. Zhou *et al.*, “The Nuclear Orphan Receptor NR2F6 Promotes Hepatic Steatosis through  
593 Upregulation of Fatty Acid Transporter CD36,” *Adv. Sci.*, 2020, doi: 10.1002/advs.202002273.

- 594 [11] H. Li *et al.*, “Nuclear orphan receptor NR2F6 confers cisplatin resistance in epithelial ovarian  
595 cancer cells by activating the Notch3 signaling pathway,” *Int. J. Cancer*, 2019, doi: 10.1002/ijc.32293.
- 596 [12] N. Hermann-Kleiter *et al.*, “Nuclear orphan receptor NR2F6 directly antagonizes NFAT and  
597 ROR $\gamma$ t binding to the Il17a promoter,” *J. Autoimmun.*, 2012, doi: 10.1016/j.jaut.2012.07.007.
- 598 [13] V. Klepsch *et al.*, “Nuclear receptor NR2F6 inhibition potentiates responses to PD-L1/PD-1  
599 cancer immune checkpoint blockade,” *Nat. Commun.*, 2018, doi: 10.1038/s41467-018-04004-2.
- 600 [14] Y. Zhao *et al.*, “‘Stripe’ transcription factors provide accessibility to co-binding partners in  
601 mammalian genomes.,” *Mol. Cell*, vol. 82, no. 18, pp. 3398-3411.e11, Sep. 2022, doi:  
602 10.1016/j.molcel.2022.06.029.
- 603 [15] L. Al-Khalili, D. Krämer, P. Wretenberg, and A. Krook, “Human skeletal muscle cell  
604 differentiation is associated with changes in myogenic markers and enhanced insulin-mediated MAPK  
605 and PKB phosphorylation,” *Acta Physiol. Scand.*, 2004, doi: 10.1111/j.1365-201X.2004.01259.x.
- 606 [16] H. N. Araujo *et al.*, “Regulation of Lin28a-miRNA let-7b-5p pathway in skeletal muscle cells  
607 by peroxisome proliferator-activated receptor delta,” *Am. J. Physiol. - Cell Physiol.*, 2020, doi:  
608 10.1152/ajpcell.00233.2020.
- 609 [17] C. L. Andersen, J. L. Jensen, and T. F. Ørntoft, “Normalization of real-time quantitative  
610 reverse transcription-PCR data: A model-based variance estimation approach to identify genes suited  
611 for normalization, applied to bladder and colon cancer data sets,” *Cancer Res.*, 2004, doi:  
612 10.1158/0008-5472.CAN-04-0496.
- 613 [18] K. J. Livak and T. D. Schmittgen, “Analysis of relative gene expression data using real-time  
614 quantitative PCR and the 2- $\Delta\Delta$ CT method,” *Methods*, 2001, doi: 10.1006/meth.2001.1262.
- 615 [19] A. M. Bolger, M. Lohse, and B. Usadel, “Trimmomatic: A flexible trimmer for Illumina  
616 sequence data,” *Bioinformatics*, 2014, doi: 10.1093/bioinformatics/btu170.
- 617 [20] R. Harmancey, D. L. Haight, K. A. Watts, and H. Taegtmeier, “Chronic hyperinsulinemia  
618 causes selective insulin resistance and down-regulates uncoupling protein 3 (ucp3) through the

- 619 activation of sterol regulatory element-binding protein (srebp)-1 transcription factor in the mouse  
620 heart,” *J. Biol. Chem.*, 2015, doi: 10.1074/jbc.M115.673988.
- 621 [21] C. Handschin, J. Rhee, J. Lin, P. T. Tarr, and B. M. Spiegelman, “An autoregulatory loop  
622 controls peroxisome proliferator-activated receptor  $\gamma$  coactivator 1 $\alpha$  expression in muscle,” *Proc. Natl.*  
623 *Acad. Sci. U. S. A.*, 2003, doi: 10.1073/pnas.1232352100.
- 624 [22] T. I. Lima and L. R. Silveira, “A microplate assay for measuring cell death in C2C12 cells,”  
625 *Biochem. Cell Biol.*, 2018, doi: 10.1139/bcb-2018-0005.
- 626 [23] M. Warnecke, H. Oster, J. Revelli, G. Alvarez-bolado, and G. Eichele, “Abnormal  
627 development of the locus coeruleus in,” *Genes Dev.*, 2005, doi: 10.1101/gad.317905.mice.
- 628 [24] N. Hermann-Kleiter *et al.*, “The Nuclear Orphan Receptor NR2F6 Is a Central Checkpoint for  
629 Cancer Immune Surveillance,” *Cell Rep.*, 2015, doi: 10.1016/j.celrep.2015.08.035.
- 630 [25] P. Kaliman, F. Viñals, X. Testar, M. Palacín, and A. Zorzano, “Phosphatidylinositol 3-kinase  
631 inhibitors block differentiation of skeletal muscle cells,” *J. Biol. Chem.*, 1996, doi:  
632 10.1074/jbc.271.32.19146.
- 633 [26] P. Rochard *et al.*, “Mitochondrial activity is involved in the regulation of myoblast  
634 differentiation through myogenin expression and activity of myogenic factors,” *J. Biol. Chem.*, 2000,  
635 doi: 10.1074/jbc.275.4.2733.
- 636 [27] O. Halevy *et al.*, “Correlation of terminal cell cycle arrest of skeletal muscle with induction of  
637 p21 by MyoD,” *Science (80-. )*, 1995, doi: 10.1126/science.7863327.
- 638 [28] I. L. De la Serna, K. Roy, K. A. Carlson, and A. N. Imbalzano, “MyoD Can Induce Cell Cycle  
639 Arrest but Not Muscle Differentiation in the Presence of Dominant Negative SWI/SNF Chromatin  
640 Remodeling Enzymes,” *J. Biol. Chem.*, 2001, doi: 10.1074/jbc.M107281200.
- 641 [29] Y. Kobayashi *et al.*, “Cyclin-Dependent Kinase 1 Is Essential for Muscle Regeneration and  
642 Overload Muscle Fiber Hypertrophy,” *Front. Cell Dev. Biol.*, 2020, doi: 10.3389/fcell.2020.564581.
- 643 [30] T. Sato, T. Yamamoto, and A. Sehara-Fujisawa, “MiR-195/497 induce postnatal quiescence of

- 644 skeletal muscle stem cells,” *Nat. Commun.*, 2014, doi: 10.1038/ncomms5597.
- 645 [31] J. M. Zhang, Q. Wei, X. Zhao, and B. M. Paterson, “Coupling of the cell cycle and myogenesis  
646 through the cyclin D1-dependent interaction of MyoD with cdk4,” *EMBO J.*, 1999, doi:  
647 10.1093/emboj/18.4.926.
- 648 [32] A. M. Abdelmoez *et al.*, “Comparative profiling of skeletal muscle models reveals  
649 heterogeneity of transcriptome and metabolism,” *Am. J. Physiol. - Cell Physiol.*, 2020, doi:  
650 10.1152/ajpcell.00540.2019.
- 651 [33] I. Casimiro, N. D. Stull, S. A. Tersey, and R. G. Mirmira, “Phenotypic sexual dimorphism in  
652 response to dietary fat manipulation in C57BL/6J mice,” *J. Diabetes Complications*, 2021, doi:  
653 10.1016/j.jdiacomp.2020.107795.
- 654 [34] T. I. Lima *et al.*, “Role of NCoR1 in mitochondrial function and energy metabolism,” *Cell*  
655 *Biology International*. 2018. doi: 10.1002/cbin.10973.
- 656 [35] T. I. Lima *et al.*, “Opposing action of NCoR1 and PGC-1 $\alpha$  in mitochondrial redox  
657 homeostasis,” *Free Radic. Biol. Med.*, 2019, doi: 10.1016/j.freeradbiomed.2019.08.006.
- 658 [36] V. A. Narkar *et al.*, “AMPK and PPAR $\delta$  Agonists Are Exercise Mimetics,” *Cell*, 2008, doi:  
659 10.1016/j.cell.2008.06.051.
- 660 [37] P. M. Badin *et al.*, “Exercise-like effects by Estrogen-related receptor-gamma in muscle do not  
661 prevent insulin resistance in db/db mice,” *Sci. Rep.*, 2016, doi: 10.1038/srep26442.
- 662 [38] D. Taillandier and C. Polge, “Skeletal muscle atrogenes: From rodent models to human  
663 pathologies,” *Biochimie*. 2019. doi: 10.1016/j.biochi.2019.07.014.
- 664 [39] D. G. Allen, G. D. Lamb, and H. Westerblad, “Skeletal muscle fatigue: Cellular mechanisms,”  
665 *Physiological Reviews*. 2008. doi: 10.1152/physrev.00015.2007.
- 666 [40] D. R. Dietrich, “Toxicological and pathological applications of proliferating cell nuclear  
667 antigen (PCNA), a novel endogenous marker for cell proliferation,” *Crit. Rev. Toxicol.*, 1993, doi:  
668 10.3109/10408449309104075.

- 669 [41] N. A. M. Pansters *et al.*, “Muscle-specific GSK-3 $\beta$  ablation accelerates regeneration of disuse-  
670 atrophied skeletal muscle,” *Biochim. Biophys. Acta - Mol. Basis Dis.*, 2015, doi:  
671 10.1016/j.bbadis.2014.12.006.
- 672 [42] I. Michailovici *et al.*, “Nuclear to cytoplasmic shuttling of ERK promotes differentiation of  
673 muscle stem/progenitor cells,” *Dev.*, 2014, doi: 10.1242/dev.107078.
- 674 [43] N. C. Jones, Y. V. Fedorov, R. S. Rosenthal, and B. B. Olwin, “ERK1/2 is required for  
675 myoblast proliferation but is dispensable for muscle gene expression and cell fusion,” *J. Cell. Physiol.*,  
676 2001, doi: 10.1002/1097-4652(200101)186:1<104::AID-JCP1015>3.0.CO;2-0.
- 677 [44] N. Hermann-Kleiter *et al.*, “The Nuclear Orphan Receptor NR2F6 Suppresses Lymphocyte  
678 Activation and T Helper 17-Dependent Autoimmunity,” *Immunity*, 2008, doi:  
679 10.1016/j.immuni.2008.06.008.
- 680 [45] W. J. Olson *et al.*, “Orphan Nuclear Receptor NR2F6 Suppresses T Follicular Helper Cell  
681 Accumulation through Regulation of IL-21,” *Cell Rep.*, 2019, doi: 10.1016/j.celrep.2019.08.024.
- 682 [46] S. L. Yang *et al.*, “The expression and biological effect of NR2F6 in non-small cell lung  
683 cancer,” *Front. Oncol.*, vol. 12, p. 940234, 2022, doi: 10.3389/fonc.2022.940234.
- 684 [47] B. Kupr, S. Schnyder, and C. Handschin, “Role of nuclear receptors in exercise-induced  
685 muscle adaptations,” *Cold Spring Harbor Perspectives in Medicine*. 2017. doi:  
686 10.1101/cshperspect.a029835.
- 687 [48] S. A. J. Verbrugge, M. Schönfelder, L. Becker, F. Y. Nezhad, M. H. de Angelis, and H.  
688 Wackerhage, “Genes whose gain or loss-of-function increases skeletal muscle mass in mice: A  
689 systematic literature review,” *Frontiers in Physiology*. 2018. doi: 10.3389/fphys.2018.00553.
- 690 [49] A. Mayeuf-Louchart *et al.*, “Rev-erb- $\alpha$  regulates atrophy-related genes to control skeletal  
691 muscle mass,” *Sci. Rep.*, 2017, doi: 10.1038/s41598-017-14596-2.
- 692 [50] H. Yamamoto *et al.*, “NCoR1 is a conserved physiological modulator of muscle mass and  
693 oxidative function,” *Cell*, vol. 147, no. 4, pp. 827–839, 2011, doi: 10.1016/j.cell.2011.10.017.

- 694 [51] N. Shimizu *et al.*, “A muscle-liver-fat signalling axis is essential for central control of adaptive  
695 adipose remodelling,” *Nat. Commun.*, 2015, doi: 10.1038/ncomms7693.
- 696 [52] D. Avram *et al.*, “Heterodimeric interactions between chicken ovalbumin upstream promoter-  
697 transcription factor family members ARP1 and Ear2,” *J. Biol. Chem.*, 1999, doi:  
698 10.1074/jbc.274.20.14331.
- 699 [53] H.-J. Lee *et al.*, “Dysregulation of nuclear receptor COUP-TFII impairs skeletal muscle  
700 development OPEN”, doi: 10.1038/s41598-017-03475-5.
- 701 [54] X. Xie, S. Y. Tsai, and M. J. Tsai, “COUP-TFII regulates satellite cell function and muscular  
702 dystrophy,” *J. Clin. Invest.*, 2016, doi: 10.1172/JCI87414.
- 703 [55] M. A. Pearen *et al.*, “The nuclear receptor, Nor-1, markedly increases type II oxidative muscle  
704 fibers and resistance to fatigue,” *Mol. Endocrinol.*, 2012, doi: 10.1210/me.2011-1274.
- 705 [56] W. Chen, X. Zhang, K. Birsoy, and R. G. Roeder, “A muscle-specific knockout implicates  
706 nuclear receptor coactivator MED1 in the regulation of glucose and energy metabolism,” *Proc. Natl.*  
707 *Acad. Sci. U. S. A.*, 2010, doi: 10.1073/pnas.1005626107.
- 708 [57] A. Seth *et al.*, “The Transcriptional Corepressor RIP140 Regulates Oxidative Metabolism in  
709 Skeletal Muscle,” *Cell Metab.*, 2007, doi: 10.1016/j.cmet.2007.08.004.
- 710 [58] C. Son *et al.*, “Reduction of diet-induced obesity in transgenic mice overexpressing uncoupling  
711 protein 3 in skeletal muscle,” *Diabetologia*, 2004, doi: 10.1007/s00125-003-1272-8.
- 712 [59] J. Darcy MacLellan, M. F. Gerrits, A. Gowing, P. J. S. Smith, M. B. Wheeler, and M. E.  
713 Harper, “Physiological increases in uncoupling protein 3 augment fatty acid oxidation and decrease  
714 reactive oxygen species production without uncoupling respiration in muscle cells,” *Diabetes*, 2005,  
715 doi: 10.2337/diabetes.54.8.2343.
- 716 [60] J. C. Clapham *et al.*, “Mice overexpressing human uncoupling protein-3 in skeletal muscle are  
717 hyperphagic and lean,” *Nature*, 2000, doi: 10.1038/35019082.
- 718 [61] C. Son *et al.*, “Up-regulation of uncoupling protein 3 gene expression by fatty acids and

- 719 agonists for PPARs in L6 myotubes,” *Endocrinology*, 2001, doi: 10.1210/endo.142.10.8446.
- 720 [62] D. S. Weigle *et al.*, “Elevated free fatty acids induce uncoupling protein 3 expression in  
721 muscle: A potential explanation for the effect of fasting,” *Diabetes*, 1998, doi: 10.2337/diab.47.2.298.
- 722 [63] A. J. Cruz-Jentoft and A. A. Sayer, “Sarcopenia,” *The Lancet*. 2019. doi: p.
- 723 [64] A. Picca *et al.*, “Update on mitochondria and muscle aging: All wrong roads lead to  
724 sarcopenia,” *Biological Chemistry*. 2018. doi: 10.1515/hsz-2017-0331.
- 725 [65] M. Bakay *et al.*, “Nuclear envelope dystrophies show a transcriptional fingerprint suggesting  
726 disruption of Rb-MyoD pathways in muscle regeneration,” *Brain*, 2006, doi: 10.1093/brain/awl023.
- 727 [66] S. Salinas, C. Proukakis, A. Crosby, and T. T. Warner, “Hereditary spastic paraplegia: clinical  
728 features and pathogenetic mechanisms,” *The Lancet Neurology*. 2008. doi: 10.1016/S1474-  
729 4422(08)70258-8.
- 730 [67] J. K. Fink, “Hereditary spastic paraplegia: Clinico-pathologic features and emerging molecular  
731 mechanisms,” *Acta Neuropathologica*. 2013. doi: 10.1007/s00401-013-1115-8.
- 732 [68] V. Klepsch *et al.*, “Nuclear orphan receptor NR2F6 as a safeguard against experimental murine  
733 colitis,” *Gut*, 2018, doi: 10.1136/gutjnl-2016-313466.
- 734 [69] L. Pelletier *et al.*, “In vivo RyR1 reduction in muscle triggers a core-like myopathy,” *Acta*  
735 *Neuropathol. Commun.*, 2020, doi: 10.1186/s40478-020-01068-4.
- 736 [70] I. Sakakibara *et al.*, “Myofiber androgen receptor increases muscle strength mediated by a  
737 skeletal muscle splicing variant of Mylk4,” *iScience*, 2021, doi: 10.1016/j.isci.2021.102303.
- 738 [71] N. K. L. Lee and H. E. Maclean, “Polyamines, androgens, and skeletal muscle hypertrophy,”  
739 *Journal of Cellular Physiology*. 2011. doi: 10.1002/jcp.22569.
- 740 [72] M. Cervelli, A. Leonetti, G. Duranti, S. Sabatini, R. Ceci, and P. Mariottini, “Skeletal Muscle  
741 Pathophysiology: The Emerging Role of Spermine Oxidase and Spermidine,” *Med. Sci.*, 2018, doi:  
742 10.3390/medsci6010014.
- 743 [73] L. Wang, H. Long, Q. Zheng, X. Bo, X. Xiao, and B. Li, “Circular RNA circRHOT1 promotes

- 744 hepatocellular carcinoma progression by initiation of NR2F6 expression,” *Mol. Cancer*, 2019, doi:  
745 10.1186/s12943-019-1046-7.
- 746 [74] J. Liu, T. Li, and X. L. Liu, “DDA1 is induced by NR2F6 in ovarian cancer and predicts poor  
747 survival outcome,” *Eur. Rev. Med. Pharmacol. Sci.*, 2017.
- 748 [75] E. T. Weatherford, X. Liu, and C. D. Sigmund, “Regulation of renin expression by the orphan  
749 nuclear receptors Nr2f2 and Nr2f6,” *Am. J. Physiol. - Ren. Physiol.*, 2012, doi:  
750 10.1152/ajprenal.00362.2011.
- 751 [76] K. Chu and H. H. Zingg, “The nuclear orphan receptors COUP-TFII and Ear-2 act as silencers  
752 of the human oxytocin gene promoter,” *J. Mol. Endocrinol.*, 1997, doi: 10.1677/jme.0.0190163.
- 753 [77] C. Jin, L. Xiao, Z. Zhou, Y. Zhu, G. Tian, and S. Ren, “MiR-142-3p suppresses the  
754 proliferation, migration and invasion through inhibition of NR2F6 in lung adenocarcinoma,” *Hum.*  
755 *Cell*, 2019, doi: 10.1007/s13577-019-00258-0.
- 756 [78] S. Raichur, P. Lau, B. Staels, and G. E. O. Muscat, “Retinoid-related orphan receptor  $\gamma$   
757 regulates several genes that control metabolism in skeletal muscle cells: Links to modulation of  
758 reactive oxygen species production,” *J. Mol. Endocrinol.*, 2007, doi: 10.1677/jme.1.00010.
- 759 [79] J. Iqbal *et al.*, “Deletion of retinoic acid-related orphan receptor gamma reduces body weight  
760 and hepatic lipids in mice by modulating the expression of lipid metabolism genes,” *Vessel Plus*, 2019,  
761 doi: 10.20517/2574-1209.2019.28.
- 762 [80] Y. Fang, H. Yu, X. Liang, J. Xu, and X. Cai, “Chk1-induced CCNB1 overexpression promotes  
763 cell proliferation and tumor growth in human colorectal cancer,” *Cancer Biol. Ther.*, 2014, doi:  
764 10.4161/cbt.29691.
- 765 [81] V. Huang *et al.*, “Upregulation of Cyclin B1 by miRNA and its implications in cancer,”  
766 *Nucleic Acids Res.*, 2012, doi: 10.1093/nar/gkr934.
- 767 [82] B. Bao, X. Yu, and W. Zheng, “MiR-139-5p Targeting CCNB1 Modulates Proliferation,  
768 Migration, Invasion and Cell Cycle in Lung Adenocarcinoma,” *Mol. Biotechnol.*, 2022, doi:

769 10.1007/s12033-022-00465-5.

770 [83] V. K. Rao *et al.*, “G9a promotes proliferation and inhibits cell cycle exit during myogenic  
771 differentiation,” *Nucleic Acids Res.*, 2016, doi: 10.1093/nar/gkw483.

772 [84] J. D. R. Knight and R. Kothary, “The myogenic kinome: Protein kinases critical to mammalian  
773 skeletal myogenesis,” *Skeletal Muscle*. 2011. doi: 10.1186/2044-5040-1-29.

774 [85] H. Tajsharghi and A. Oldfors, “Myosinopathies: Pathology and mechanisms,” *Acta*  
775 *Neuropathologica*. 2013. doi: 10.1007/s00401-012-1024-2.

776 [86] S. Schiaffino, “Muscle fiber type diversity revealed by anti-myosin heavy chain antibodies,”  
777 *FEBS Journal*. 2018. doi: 10.1111/febs.14502.

778

779

## 780 FIGURES LEGENDS

### 781 **Figure 1. Nr2f6 knockdown derepresses the expression of genes involved in metabolism and**

782 **myogenesis. (A)** Volcano plot of Nr2f6 knockdown C2C12 myocytes. Genes upregulated in red and

783 downregulated in blue (FDR <0.05, log<sub>2</sub>FC >0.5). N=4-5. **(B)** Network of ontology terms enriched in the

784 differentially expressed genes. Groups of similar terms were manually curated and encircled as

785 indicated. **(C, D)** Gene ontology enrichment of downregulated and upregulated genes. **(E)** Panel of

786 myogenic differentiation markers differentially regulated by Nr2f6 knockdown with Myogenic

787 Regulatory Factors (MRFs) and myosin isoforms with their respective fiber expression pattern[85], [86].

788 **(F)** Insulin signaling pathway schematic displaying differentially expressed genes after Nr2f6

789 knockdown and other components of the pathway. Metabolites are depicted in yellow borders and

790 unchanged genes are in orange borders. **(G)** Gene expression measured by RT-qPCR of markers of

791 myogenic differentiation in primary human skeletal muscle cells transfected with control non-target

792 RNAi (siScr) or siNr2f6. N = 5-6. Boxplot with whiskers spanning minimum to maximal and box edges

793 25<sup>th</sup>-75<sup>th</sup> percentile, the line at the median and + at the mean. \* Indicates p < 0.05 using unpaired two-

794 tailed Student's t-test.

### 795 **Figure 2. Nr2f6 depletion increases fatty acid oxidation and protects cells against lipid-induced**

796 **stress. (A)** Fatty-acid-dependent oxygen consumption assay in control siScr and siNr2f6 C2C12

797 myocytes. Data displayed as mean ±SD. On the right, calculated respiratory parameters are displayed as

798 a line on the mean and minimum to max bars. N = 3. \* Indicates p < 0.05 using unpaired two-tailed

799 Student's t-test. **(B)** Oligomycin-induced extracellular acidification rate during a high-glucose oxygen

800 consumption assay. N=4. **(C)** Lactate measurement in cell culture media of C2C12 myocytes transfected

801 with control siScr and siNr2f6. N=3. **(D, E)** Relative gene expression using RT-qPCR in stable Nr2f6

802 knockdown (shNr2f6) C2C12 cells and control shGFP stable cells. **(F)** Cell death as measured by

803 propidium iodide in control (shGFP) and shNr2f6 myocytes following treatment with 500 μM palmitate

804 for 20 hours. N=3. **(G, H)** Mitochondrial and total superoxide production following palmitate treatment

805 in shGFP and shNr2f6 stable C2C12 cells. N=3-4. **(I)** Relative Nr2f6 mRNA expression in C2C12  
806 myotubes treated with 500  $\mu$ M palmitate or vehicle for 20 hours. N=3. **(J)** Relative Nr2f6 mRNA  
807 expression in the gastrocnemius of mice undergoing a control chow or high-fat diet for 16 weeks. N=7.  
808 **(K)** Densitometry and representative western blot image of Nr2f6 in gastrocnemius lysates from mice  
809 fed HFD or control chow for 16 weeks. N=6. Boxplot with whiskers spanning minimum to maximal and  
810 box edges 25<sup>th</sup>-75<sup>th</sup> percentile, the line at the median and + at the mean. \* Indicates  $p < 0.05$  using  
811 unpaired two-tailed Student's t-test.

812 **Figure 3. Nr2f6 directly regulates PGC1-a and UCP3 gene expression.** **(A)** Relative gene expression  
813 using RT-qPCR in stable Nr2f6-myc overexpression myotubes. N=4-5. **(B)** Densitometry and  
814 representative images of PGC-1 $\alpha$  western blot in stable Nr2f6-myc overexpression myotubes. N=5. **(C)**  
815 Relative gene expression using RT-qPCR in stable Nr2f6 knockdown myotubes. N=3-5. **(D)** Luciferase  
816 reporter assay in HEK293 cells with 2 kbp PGC1A promoter overexpressing HA-tagged Nr2f6 or  
817 control empty vector (EV). **(E)** Luciferase activity of UCP3 promoter transactivation assay in cells  
818 overexpressing Nr2f6-myc and siNr2f6 transfected cells. N=3. **(F)** Mouse UCP3 genomic locus  
819 retrieved from UCSC Genome Browser with the Nr2f6 response element highlighted. Top tracks: ChIP-  
820 seq of Myogenin and MyoD at 24h and 60h of differentiation. Middle track: DNase hypersensitivity  
821 assay, with open sensitive regions in grey. Bottom tracks: histone marks ChIP-seq. **(G)** Relative gene  
822 expression using RT-qPCR in human primary skeletal myotubes transfected with siNr2f6 or siScr. N=6.  
823 Boxplot with whiskers spanning minimum to maximal and box edges 25<sup>th</sup>-75<sup>th</sup> percentile, the line at the  
824 median and + at the mean. \* Indicates  $p < 0.05$  using unpaired two-tailed Student's t-test. The numbers  
825 above some bars indicate the p-value.

826 **Figure 4. The molecular signature of Nr2f6 overexpression in skeletal muscle reveals an increase**  
827 **in inflammation and a decrease in muscle contraction and metabolism.** **(A)** Heat-map of top 30  
828 most modulated genes in *tibialis anterior* muscle electroporated with empty vector (control) or an Nr2f6  
829 coding plasmid. N=4. **(B, C)** Gene ontology enrichment of downregulated and upregulated genes. **(D, E,**

830 **F)** Validation of selected markers modulated in the microarray by RT-qPCR. N=4. Insert on D:  
831 representative western blot for validation of Nr2f6 protein content in *tibialis anterior* samples under  
832 control and electroporated conditions. Boxplot with whiskers spanning minimum to maximal and box  
833 edges 25<sup>th</sup>-75<sup>th</sup> percentile, the line at the median and + at the mean. \* Indicates  $p < 0.05$  using unpaired  
834 two-tailed Student's t-test. The numbers above some bars indicate the p-value.

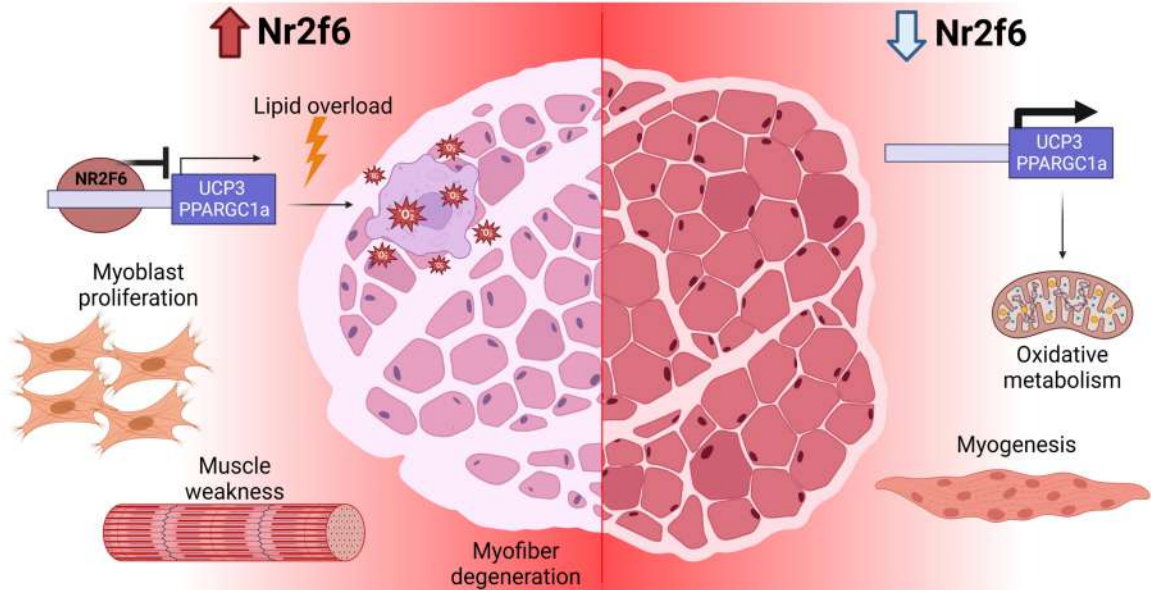
835 **Figure 5. Overexpression of Nr2f6 induces muscle atrophy and impairs muscle force production.**

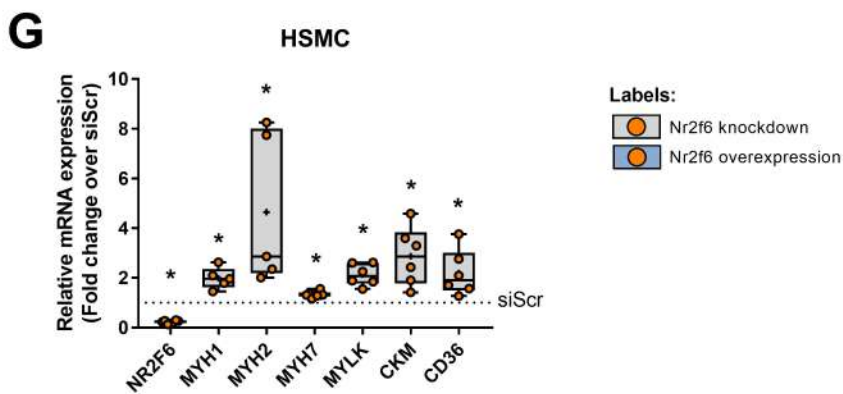
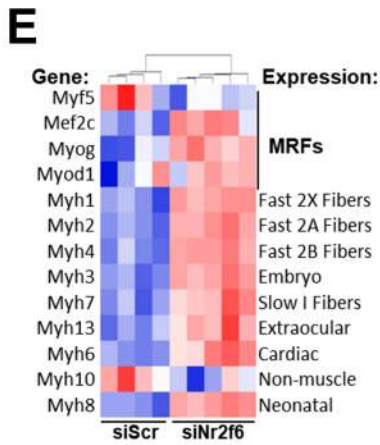
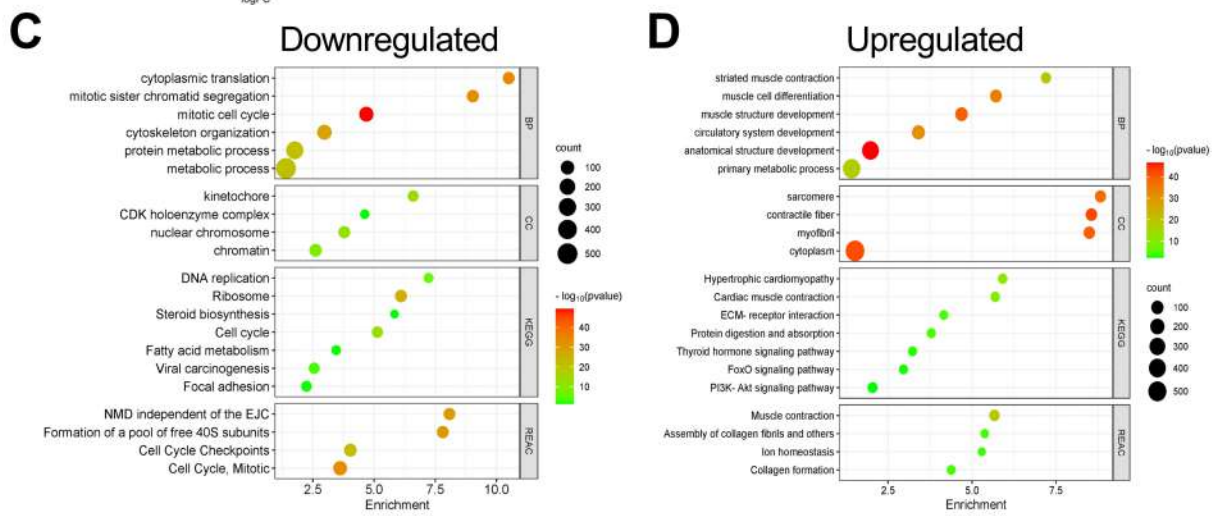
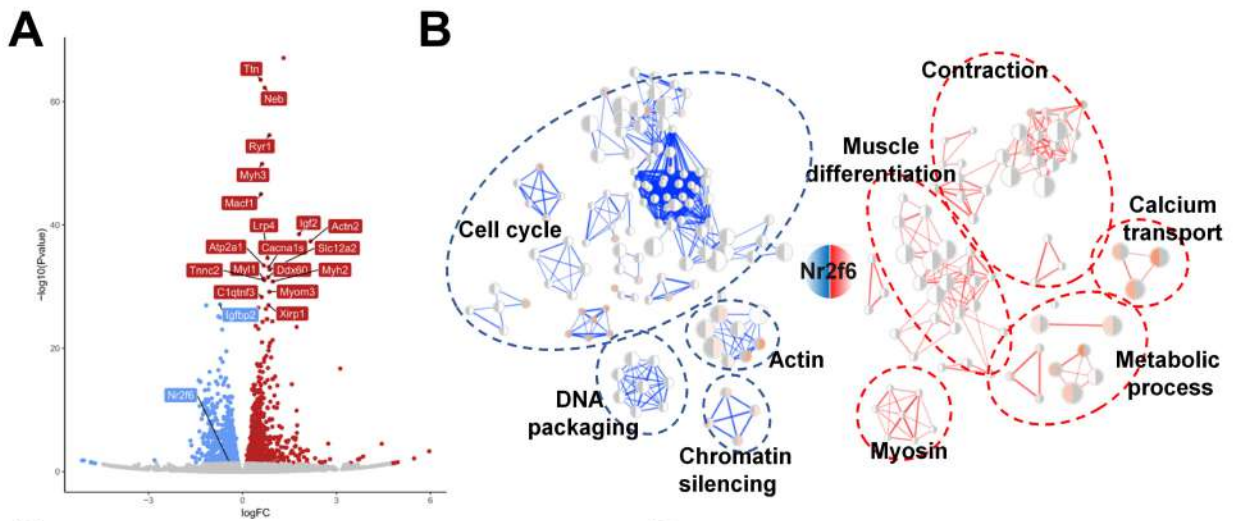
836 **(A)** Weight of *tibialis anterior* muscles (TA) electroporated with empty vector or Nr2f6 coding plasmid.  
837 Top: representative photo. N=12. **(B)** Representative images of myosin heavy chain staining in the  
838 electroporated TAs for fiber type determination. In green, MHC IIA; in red, MHC IIB; unstained fibers  
839 as IIX. No significant number of MHCI fibers were stained, therefore the corresponding channel was  
840 omitted. N=7. **(C, D)** Total and type-segmented number of fibers. N=7. **(E)** *Ex-vivo* contraction maximal  
841 force production in FDB muscles electroporated with control empty vector (EV) or Nr2f6 coding  
842 plasmid. N=5. Data are displayed as individual animals and bars at the mean. \* Indicates  $p < 0.05$  using  
843 ratio paired two-tailed Student's t-test.

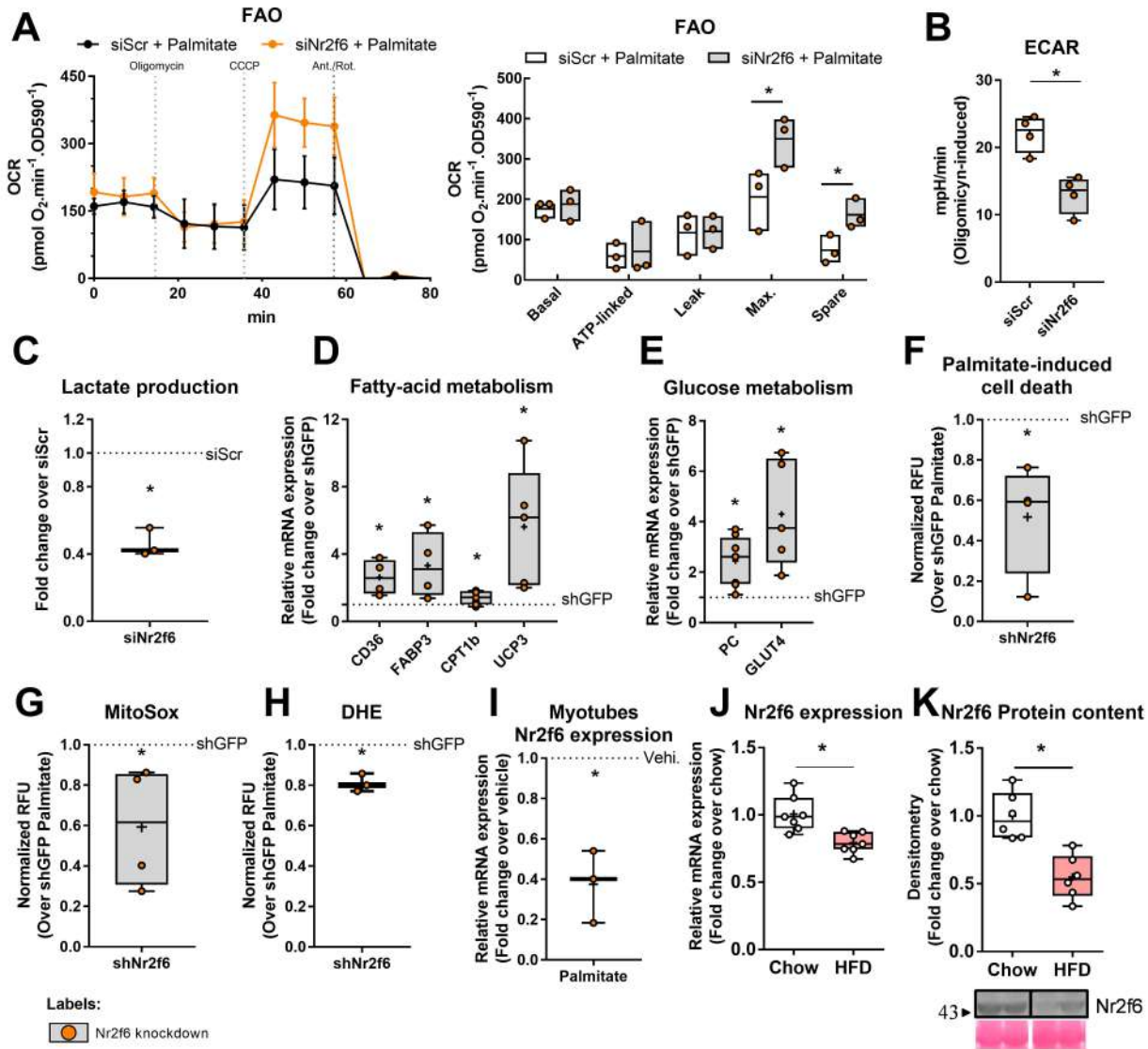
844 **Figure 6. Nr2f6 promotes myoblast proliferation. (A)** Scatter plot of differentially expressed genes in  
845 Nr2f6 knockdown in C2C12 myocytes and Nr2f6 overexpression in mice TA. In red: genes upregulated  
846 by Nr2f6; in blue: genes downregulated by Nr2f6; in grey: genes with the same direction of modulation  
847 by Nr2f6 overexpression and knockdown. **(B)** Interaction network of genes consistently regulated by  
848 Nr2f6 overexpression and knockdown and with detected Nr2f6 binding motif at the promoter region. In  
849 blue: genes downregulated; in red: genes upregulated. The number of connections of each gene  
850 increases clockwise. **(C, D)** Representative images of western blot of the electroporated *tibialis anterior*  
851 and densitometric quantitation of protein bands. N=4. **(E, G)** Proliferation curves of stable Nr2f6  
852 knockdown and overexpression cell lines and the calculated doubling time. **(F, H)** RT-qPCR of cell  
853 cycle arrest markers in Nr2f6 knockdown and overexpression stable cell lines, respectively. N=4-6.  
854 Boxplot with whiskers spanning minimum to maximal and box edges 25<sup>th</sup>-75<sup>th</sup> percentile, the line at the

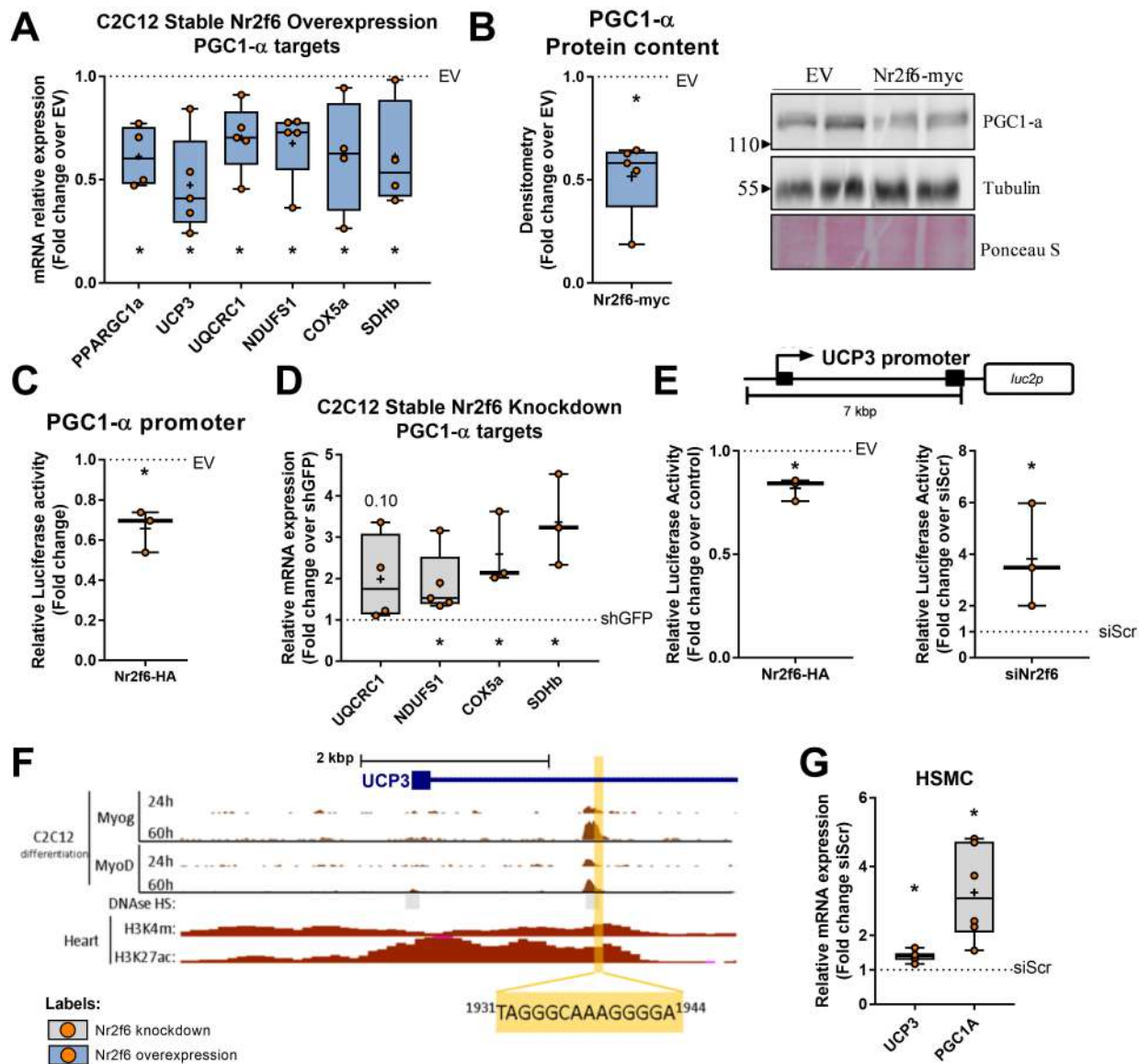
855 median and + at the mean. \* Indicates  $p < 0.05$  using unpaired two-tailed Student's t-test. The numbers  
856 above some bars indicate the p-value.

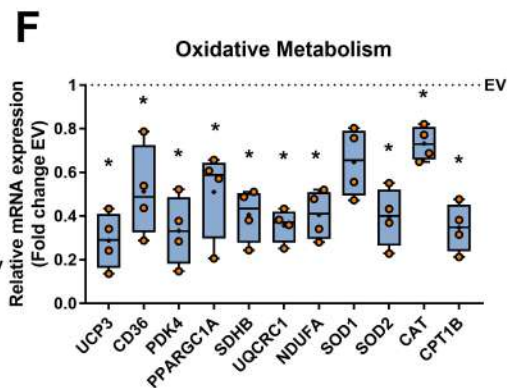
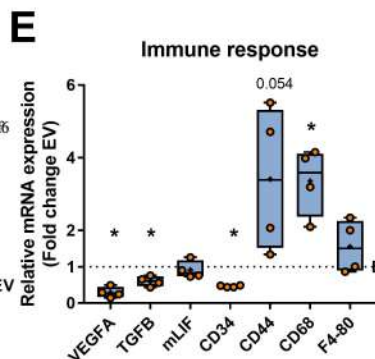
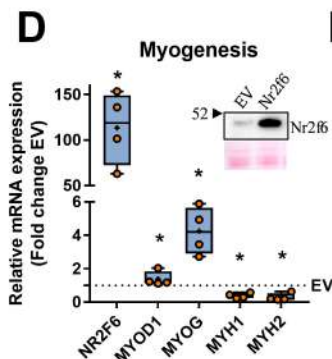
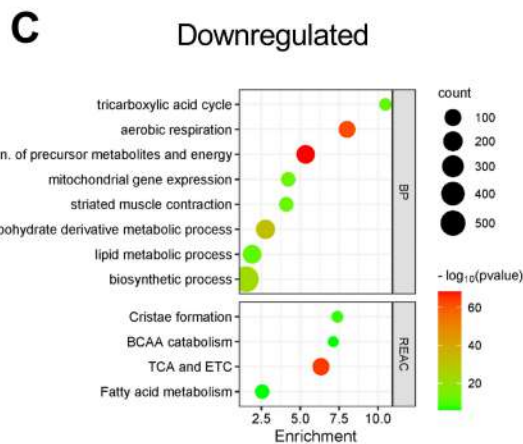
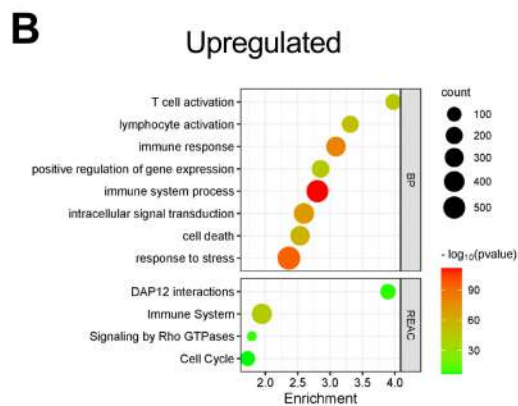
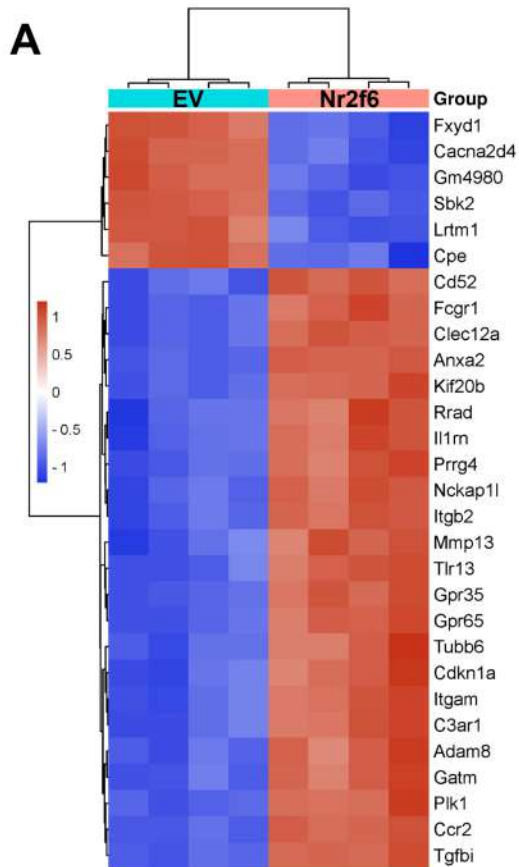
857 **Figure 7. Nr2f6 represses core genes of muscle contraction.** Nr2f6 overexpression reduces the  
858 expression of several genes of the contractile apparatus, myofiber calcium handling, and action potential  
859 transduction. Genes with Nr2f6 binding motif at the promoter are underscored. Differentially expressed  
860 genes following Nr2f6 overexpression in mouse TA were selected according to ontology terms related  
861 to muscle contraction and function. The arrows indicate the up- or downregulation. Sodium Voltage-  
862 Gated Channel Alpha Subunit 4 (Scn4a), Potassium Inwardly Rectifying Channel Subfamily J Member  
863 2 (Kcnj2), Solute Carrier Family 8 Member A3 (Slc8a3), Muscle Associated Receptor Tyrosine Kinase  
864 (Musk), Ryanodine Receptor 1 (Ryr1), Calsequestrin 1 (Casq1), ATPase Sarcoplasmic/Endoplasmic  
865 Reticulum Ca<sup>2+</sup> Transporting 2 (SERCA2, Atp2a2), Cholinergic Receptor Nicotinic Alpha  
866 1/delta/gamma subunit Chrna1/d/g), Troponin T1/I1/I2/C1 (Tnnt1/Tnni1/Tnni2/c1), Myom1/2  
867 (Myomesin1/2), Myozenin1/3 (Myoz1/3), Myosin light chain kinase 2/4 (Mylk2/4), Myosin heavy  
868 chain 3 (Myh3), Myosin binding protein C1/2 (Mybpc1/2)





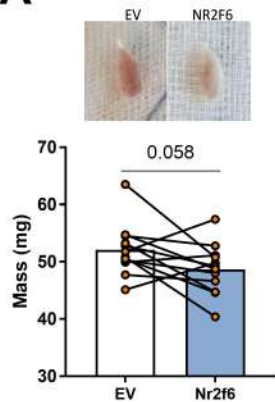
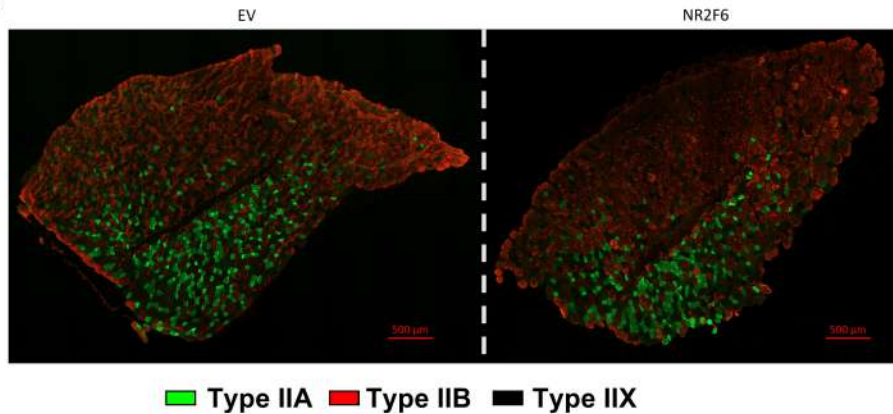
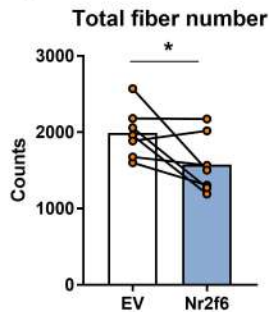
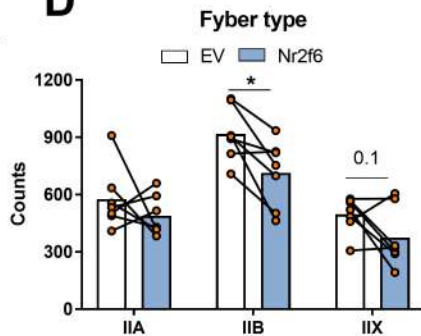






Labels:  

 Nr2f6 overexpression

**A****B****C****D****E**